

First-principles Hubbard U and Hund's J corrected approximate density-functional theory predicts an accurate fundamental gap in rutile and anatase TiO_2

Okan K. Orhan¹ and David D. O'Regan¹

¹*School of Physics, AMBER, and CRANN Institute,
Trinity College Dublin, the University of Dublin, Ireland*

Titanium dioxide (TiO_2) presents a long-standing challenge for approximate Kohn-Sham density-functional theory (KS-DFT), as well as to its Hubbard-corrected extension, DFT+ U . We find that a previously proposed extension of first-principles DFT+ U to incorporate a Hund's J correction, termed DFT+ $U+J$, in combination with parameters calculated using a recently proposed linear-response theory, predicts fundamental band-gaps accurate to well within the experimental uncertainty in rutile and anatase TiO_2 . Our approach builds upon established findings that Hubbard correction to both titanium $3d$ and oxygen $2p$ subspaces in TiO_2 , symbolically giving DFT+ $U^{d,p}$, is necessary to achieve acceptable band-gaps using DFT+ U . This requirement remains when the first-principles Hund's J is included. We also find that the calculated gap depends on the correlated subspace definition even when using subspace-specific first-principles U and J parameters. Using the simplest reasonable correlated subspace definition and underlying functional, the local density approximation, we show that high accuracy results from using a relatively uncomplicated form of the DFT+ $U+J$ functional. For closed-shell systems such as TiO_2 , we describe how various DFT+ $U+J$ functionals reduce to DFT+ U with suitably modified parameters, so that reliable band gaps can be calculated for rutile and anatase with no modifications to a conventional DFT+ U code.

I. INTRODUCTION

Titanium dioxide (TiO_2) has been widely used for several decades in diverse industrial applications such as pigmentation and coating^{1–3} due to its non-toxicity, low-cost production and thermal stability. TiO_2 came under particularly intense scrutiny with the ground-breaking work of Fujishima and Honda, who demonstrated water splitting in TiO_2 photo-chemical cells in the ultra-violet (UV) spectral range in 1972⁴. Indeed, since then, TiO_2 -based structures have been engineered for diverse optoelectronic applications such as photo-catalysts, photovoltaics, sensors, and for energy and environmental applications^{5–7}. In nature, TiO_2 has three common polymorphs: rutile, anatase, and brookite⁸. TiO_2 -rutile and TiO_2 -anatase are more common in industrial applications, as brookite is less stable and difficult to synthesize in large volumes⁹. The electronic structures of pristine TiO_2 -rutile and TiO_2 -anatase have been extensively studied experimentally^{10–14}, and the most reliable data currently available shows that TiO_2 -rutile and TiO_2 -anatase have fundamental (electronic, not optical) band gaps of 3.03 eV^{12,13} and 3.47 eV¹¹, respectively.

First-principles simulations can provide valuable insights into the electronic structures and processes at play in TiO_2 -based systems, offering clues for the engineering of these systems for desired applications. This requires the accurate description of their electronic structures in the region of their band edges, naturally, and this must necessarily be found by means of computationally feasible and scalable methods if disordered structures and diverse dopants are to be assessed in any detail. There exist numerous acceptably reliable approaches, such as quantum chemistry methods^{15,16}, hybrid-functionals¹⁷, and many-body perturbation methods^{18–20}, but these methods are too computationally demanding for routine application

to defective and disordered systems.

Density-functional theory (DFT)²¹, specifically Kohn-Sham DFT (KS-DFT)²² using (semi-)local density exchange-correlation functionals^{22–25} offers a computationally feasible framework to study the electronic structures of spatially complex TiO_2 -based systems. In the present work, with that challenge in mind, we use a linear-scaling implementation of DFT, the Order-N Electronic Total Energy Package (ONETEP)^{26–29}. However, it is well-known that semi-local KS-DFT is unable to capture the approximate magnitude of the band-gap of TiO_2 , a common observation among transition-metal oxides (TMOs) generally^{30–32}, and so it requires, at the very least, some corrective measures for reliable use.

In this work, we revisit the computationally efficient approach of applying Hubbard-model inspired corrections to approximate KS-DFT, namely DFT+ U ^{33–41} which is technically a generalized Kohn-Sham method⁴², in terms of its capability of accurately describing the fundamental electronic band gap of TiO_2 polymorphs. We find that unlike-spin Hund's J correction, specifically that introduced in the pioneering work of Ref. 43, is the key ingredient that enables the band gaps of TiO_2 to be accurately described with this method. A corrective functional is only as good as its parameters, and here we use the recently-proposed minimum-tracking linear-response formalism of Ref. 44 for calculating them. Encouragingly for practical use, moreover, we find that for closed-shell (non-spin-polarized) systems such as pristine TiO_2 and other TMOs towards the edges of the periodic table d -block, no modification to a standard DFT+ U code is needed to include Hund's J corrections.

No differently to what has been found in previous works^{45–48} and as an inevitable consequence of the O $2p$ character of the valence-band edge, in order to achieve significantly improved results using DFT+ U we need to

apply corrective potentials to oxygen 2*p* orbitals on the same footing as to titanium 3*d* orbitals. The addition of Hund's *J* does not change this fact, and irrespective of whether *J* is included we denote this two-species correction as DFT+*U*^{*d,p*}, short for DFT+*U*^{*d*}+*U*^{*p*}, following the literature. Unlike prior works on TiO₂, in which one or both of *U*^{*d*} and *U*^{*p*} was found to require empirical tuning for good results, in this work we only use first-principles calculated *U* and *J* parameters (specifically, using the minimum-tracking linear-response method^{44,49}), for both the Ti 3*d* and O 2*p* subspaces.

When the unlike-spin Hund's *J* term is included (using a particularly simple form of DFT+*U*+*J*, in agreement with the detailed analysis of Ref. 43) we predict a generalised Kohn-Sham band-gap of a better quality than that which hybrid functionals or G₀W₀ gives, for both polymorphs, when gauged against reported experimental findings (recent, high-quality ones in the case of anatase, where it seems to be more challenging to measure). The ionic geometries of both polymorphs are found to be very little affected by the force terms due to this functional form. We note in passing that both functional classes, DFT+*U* and hybrids, are differentiable in terms of the density-matrix and have a non-local potential, and so their generalised Kohn-Sham gaps include exchange-correlation derivative discontinuities⁵⁰ and are directly comparable to experiment. Promisingly for future TiO₂ simulation, and as the central conclusion of this work, we find that the same first-principles DFT+*U*^{*d,p*}+*J*^{*d,p*} functional predicts the experimental fundamental gap to within the uncertainty of the experiment, for both polymorphs.

II. METHODOLOGY

Perhaps the most well-known systematic error exhibited by conventional approximate functionals in KS-DFT is the self-interaction error (SIE)^{51–55}, and its many-body generalization, the delocalization error^{56–62}. SIE arises due to spurious self-repulsion of electronic density in the KS-DFT formalism and it also persists, albeit often to a lesser extent, within generalized Kohn-Sham schemes. While the origins of SIE are well understood, it is hard to avoid it in the construction of closed-form approximate functionals. SIE leads to the well-known significant, even drastic underestimation of fundamental band gaps of TMOs in particular^{30–32}, and TiO₂-rutile and TiO₂-anatase are no exception in this regard⁶³. Less well understood is the generalization of SIE to account for the spin degree of freedom, which is not necessarily less relevant in closed-shell systems where the spin happens to evaluate to zero. In this section, we outline in detail our methodology for computing and incorporating parameters, the Hubbard *U*^{*d,p*} for density-related error and Hund's *J*^{*d,p*} for spin-related error, to correct a very low-cost density functional for the specific case of TiO₂.

A. DFT+*U*+*J* functionals and their simplification for closed-shell systems

DFT+*U* is routinely applied to correct for SIE, particularly for the spurious delocalization of electronic states associated with transition-metal 3*d* orbitals. The DFT+*U* total energy is given by

$$E_{\text{DFT}+U} = E_{\text{DFT}} + E_U, \quad (1)$$

where the rotationally-invariant form of *E_U* for a given SIE-prone subspace^{30,38,64}, particularly if we take its relatively recent DFT+*U*+*J* form of Ref. 43, is given by

$$E_U[\{n^\sigma\}] = \frac{1}{2} \sum_{\sigma} \sum_{m,m'} \left\{ \underbrace{U [n_{mm'}^{\sigma} \delta_{m'm} - n_{mm'}^{\sigma} n_{m'm}^{\sigma}]}_{\text{I}} - \underbrace{J [n_{mm'}^{\sigma} \delta_{m'm} - n_{mm'}^{\sigma} n_{m'm}^{\sigma}]}_{\text{II}} + \underbrace{J [n_{mm'}^{\sigma} n_{m'm}^{\bar{\sigma}}]}_{\text{III}} - \underbrace{2J [\delta^{\sigma\sigma_{\min}} n_{mm'}^{\sigma} \delta_{m'm}]}_{\text{IV}} \right\}. \quad (2)$$

Here, σ is a spin index, $\bar{\sigma}$ is the corresponding opposite spin, σ_{\min} is the index of the minority-population spin channel for the subspace at hand, $n_{mm'}$ is the subspace-projected KS density-matrix. The Hubbard *U* is, in this work at least, interpreted as the subspace-and-spin-averaged net Hartree-plus-exchange-correlation interaction. Hund's *J* is its spin-splitting counterpart. We will presently detail what, precisely, is meant by spin-averaging and spin-splitting in this context.

The choice of appropriate form of DFT+*U*(+*J*) energy functional depends on various factors such as the system under consideration, the limitations and robustness of approaches to determine the Hubbard *U* and Hund's *J* parameters, and the underlying approximate density functional. For instance, it was argued in Ref. 43 that term (IV), which we dub the 'minority spin term', is best not included, as it arises due to the double-counting correction of a type of two-particle density-matrix interaction that is unlikely to be very much present in the underlying density functional. Our numerical results will support this analysis. It was furthermore found to lead to numerical instabilities, and we have also noted this effect in our own calculations. Our tentative explanation of this instability is that, when the net spin of a site is weak, the potential arising due to this term can switch over discretely from one spin channel to the other. The simplest functional form is achieved, of course, by neglecting the explicit correction of exchange and effectively by setting *J* = 0 eV. If a value for *J* is available, then so is the Dudarev functional³³, which includes only like-spin correction terms (the terms (I) and (II)) via an effective parameter, $U_{\text{eff}} = U - J$ resulting symbolically in DFT+*U*_{eff}.

Inspired by the Dudarev model, we note and primarily use in this work the fact that the full DFT+*U*+*J* functional of Eq. (2) may be applied to closed-shell systems,

without approximation, using an unmodified DFT+ U code with no J implementation. To see this clearly, we can rearrange Eq. (2) and introduce an additional parameter, α , which is exactly that α which is available and used to calculate the Hubbard U in many standard DFT+ U codes⁴⁰. Here, it captures the inclusion minority spin term (term IV), when re-writing Eq. (2) as

$$E_U = \sum_{\sigma, m, m'} \left\{ \frac{U_{\text{full}}}{2} [n_{mm'}^{\sigma} \delta_{m'm} - n_{mm'}^{\sigma} n_{m'm}^{\sigma}] + \alpha n_{mm'}^{\sigma} \delta_{m'm} \right\}, \quad (3)$$

where $U_{\text{full}} = U - 2J$. Three reasonable options for α are tested in this study, representing different interpretations of the minority spin (term IV):

1. The most natural treatment (of term IV) for closed-shell systems, that suggested in Ref. 43, is to interpret $\sigma_{\text{min}} = \sigma$, such that $\delta^{\sigma\sigma_{\text{min}}} = 1$. This requires us to set $\alpha = -J/2$.
2. A modification of the latter, intended to avoid a discontinuity in the total energy at the onset of non-zero spin polarization (it doesn't avoid such a discontinuity in the potential), is to "share" the minority spin term between the two spins, setting $\delta^{\sigma\sigma_{\text{min}}} = 1/2$ for closed-shell systems. This leads to $\alpha = 0$ and the resulting Hubbard functional is simply a Dudarev functional with $U_{\text{full}} = U - 2J$.
3. In the last case, the minority spin term is neglected, as it was argued that it is best to do in its originating Ref. 43, by setting $\delta^{\sigma\sigma_{\text{min}}} = 0$. For closed-shell systems, DFT+ $U+J$ is then recovered by DFT+ U code with parameters U_{full} and $\alpha = J/2$.

In this work, we test these different corrective functionals by application to both the Ti 3d and O 2p subspaces of TiO₂, presenting DFT+ U^d (no O 2p correction) results only for the sake of illustration and completeness. It has previously been comprehensively demonstrated, in Ref. 65, that it is not possible to reconcile a reasonable band-gap with reasonable lattice constants when applying DFT+ U only to Ti 3d subspaces in TiO₂. We further motivate our inclusion of O 2p corrections in Appendix A and with reference to Fig 3. In the Supplementary Material that accompanies this work⁶⁶, we illustrate that the favoured DFT+ $U+J$ functional (minority spin term neglected) has only a very small effect on the lattice constants and internal ionic geometries of both polymorphs predicted by the underlying functional. There, we also specify the computational parameters of our study in detail.

B. The minimum-tracking linear-response approach for first-principles Hubbard U and Hund's J parameters

The results of DFT+ $U^{d,p}$ are only as good as its input Hubbard U and Hund's J parameters. Finite-difference linear-response theory provides a practical, widely available first-principles method for calculating these^{39,40,43}. It has been found that linear-response tends to give Hubbard U parameters for closed-shell systems that are too high for practical use, and this is usually deemed to be an erroneous overestimation^{44,67–69}. The present work provides hints that these values may be correct after all, but that Hund's J effectively reduces them and so the latter is (counter-intuitively, perhaps) more important to include in closed-shell systems. If a system has zero spin polarization, the systematic error in the approximate functional related to the spin *degree of freedom* may still be large. In this work, we employed the recently-introduced minimum-tracking variant⁴⁹ of linear-response as implemented in the ONETEP DFT+ U implementation^{26,70}, and in particular, its spin-specific extension introduced in Ref. 44. The 'scaled 2×2 ' method was used here to evaluate the Hubbard U , Hund's J , and effective Hubbard U parameters ($U_{\text{eff}} = U - J$ and $U_{\text{full}} = U - 2J$) for the Ti 3d and O 2p subshells of pristine TiO₂-rutile and TiO₂-anatase using

$$U = \frac{1}{2} \frac{\lambda_U (f^{\uparrow\uparrow} + f^{\uparrow\downarrow}) + f^{\downarrow\uparrow} + f^{\downarrow\downarrow}}{\lambda_U + 1} \quad (4)$$

$$\text{and } J = -\frac{1}{2} \frac{\lambda_J (f^{\uparrow\uparrow} - f^{\uparrow\downarrow}) + f^{\downarrow\uparrow} - f^{\downarrow\downarrow}}{\lambda_J - 1}, \quad (5)$$

where

$$\lambda_U = \frac{\chi^{\uparrow\uparrow} + \chi^{\uparrow\downarrow}}{\chi^{\downarrow\uparrow} + \chi^{\downarrow\downarrow}}, \quad \text{and} \quad \lambda_J = \frac{\chi^{\uparrow\uparrow} - \chi^{\uparrow\downarrow}}{\chi^{\downarrow\uparrow} - \chi^{\downarrow\downarrow}}, \quad (6)$$

and where the projected interacting response matrices are given by $\chi^{\sigma\sigma'} = dn^{\sigma}/dv_{\text{ext}}^{\sigma'}$. The spin-dependent interaction strengths $f^{\sigma\sigma'}$ are calculated by solving 2×2 matrix equation given by

$$f = \left[\left(\frac{\delta v_{\text{KS}}}{\delta v_{\text{ext}}} - 1 \right) \left(\frac{\delta n}{\delta v_{\text{ext}}} \right)^{-1} \right], \quad (7)$$

for which matrix entities are obtained by linear fitting to small changes of the subspace occupancies δn^{σ} and subspace-averaged Kohn-Sham potentials $\delta v_{\text{KS}}^{\sigma}$ with respect to incrementally varying uniform perturbing potentials $\delta v_{\text{ext}}^{\sigma}$ on the targeted subspaces. These definitions are equivalent to a particular choice of perturbation in the more physically transparent but perturbation-independent expressions

$$U = \frac{d(v_{\text{Hxc}}^{\uparrow} + v_{\text{Hxc}}^{\downarrow})}{2d(n^{\uparrow} + n^{\downarrow})} \quad \text{and} \quad J = -\frac{d(v_{\text{Hxc}}^{\uparrow} - v_{\text{Hxc}}^{\downarrow})}{2d(n^{\uparrow} - n^{\downarrow})}, \quad (8)$$

LDA rutile	Ti ⁰ conf.		Ti ³⁺ conf.	
	Ti	O	Ti	O
U	3.56	8.57	5.59	8.57
J	0.29	0.92	0.38	0.89
$U_{\text{eff}} = U - J$	3.27	7.66	5.20	7.68
$U_{\text{full}} = U - 2J$	2.98	6.74	4.82	6.80

TABLE I. First-principles LDA-appropriate Hubbard U and Hund’s J parameters calculated using the minimum-tracking linear-response method^{49,70}, both for the Ti 3d and O 2p subspaces of TiO₂-rutile. The Ti 3d parameters depend significantly on the pseudo-atomic solver charge configuration used to construct the corresponding DFT+ U subspace, with 3+ providing a significantly more localised subspace and consequently higher parameters. Shown also are the effective Hubbard U parameter of the Dudarev model (U_{eff}) and that helps to reproduce DFT+ U + J for closed-shell systems (U_{full}).

where the factor 1/2 signifies averaging (or halving the of splitting between) the subspace averaged Hartree-plus-exchange-correlation potentials, v_{Hxc}^{σ} . Eqs. 8 can be taken as definition of minimum-tracking linear response, and if using them separately it is natural to use $\delta v_{\text{ext}}^{\uparrow} = \delta\alpha = \delta v_{\text{ext}}^{\downarrow}$ for U and $\delta v_{\text{ext}}^{\uparrow} = \delta\beta = -\delta v_{\text{ext}}^{\downarrow}$ for J .

The scaling factors become $\lambda_U = 1$ and $\lambda_J = -1$ for spin-unpolarized systems such as the pristine TiO₂-rutile and TiO₂-anatase. This reflects the vanishing linear coupling between subspace occupancy and magnetization in such systems. As a result, the ‘scaled 2×2 ’ method reduces to the ‘simple 2×2 ’ method⁴⁴, which can be summarized as $U = (f^{\sigma\sigma} + f^{\sigma\sigma})/2$, $J = (f^{\sigma\sigma} - f^{\sigma\sigma})/2$ (this gives a Dudarev $U_{\text{eff}} = f^{\sigma\sigma}$, which is reasonable for a like-spin-only corrective functional). In fact, time-reversal symmetry can be readily exploited for closed-shell systems, where it is sufficient to perturb one spin channel only, filling in half of the matrix elements by symmetry, e.g. $\chi^{\uparrow\uparrow} = \chi^{\downarrow\downarrow}$. This feature of the 2×2 approach enabled the *simultaneous* calculation of U and J in this work, from a single group of self-consistent calculations perturbing one spin channel only by finite-differences. We have verified numerically that Eqs. 8 provide the same results under these conditions. The response matrix elements coupling Ti 3d and O 2p subspaces are not projected out, as to include such entries in the response matrices would necessitate corresponding terms in the corrective functional (these are usually called + V), which would complicate our analysis focused on Hund’s J .

III. RESULTS AND DISCUSSION

We first present the calculated Hubbard U and Hund’s J parameters for pristine, closed-shell TiO₂-rutile and TiO₂-anatase. As a preliminary test, LDA-appropriate parameters were calculated for TiO₂-rutile with two different definitions of the DFT+ U target subspace for Ti

3d orbitals. Specifically, both neutral and 3+ (still non-spin-polarized) atomic DFT calculations were separately performed using the functionality available in ONETEP and described in Ref. 71, to generate pseudo-atomic orbitals to define the 3d subspace, and also to build the initial density and NGWF guesses. The tensorial representation⁷² was used to correctly account for the slight nonorthogonality among the orbitals for a given subspace, which arises due to their sampling in the ONETEP plane-wave-like basis. An OPIUM⁷³ norm-conserving pseudo-potential with a 3+ reference state was used for Ti, while a charge-neutral atomic configuration was used for O (OPIUM pseudo-potential generation, DFT+ U definition, and initial density and NGWF guess generation) throughout. The resulting Hubbard U and Hund’s J parameters are summarized in Table I.

We find that the calculated LDA Hubbard U value for Ti 3d increases by ~ 2 eV or $\sim 60\%$ when going from a neutral subspace configuration to a 3+ charge one, due to the pronounced increase in the spatial localization of the subspace, plotted in Fig. 3 of Appendix B. The relatively small calculated J value also increases somewhat, by a smaller amount in multiplicative terms, 30%. $U_{\text{full}} = U - 2J$ therefore also increases by $\sim 60\%$. We choose the smoother orbitals from the neutral pseudo-atomic solver configuration to define DFT+ U in our further calculations, and the reasoning for this will be discussed and demonstrated in Appendix B. There, we will see that, not only does calculating U and J from first-principles not compensate for the arbitrariness of the DFT+ U projectors in TiO₂-rutile, it in fact *reinforces* it. We note a small but nonetheless irksome deviation in the O 2p J parameter when moving to a 3+ Ti 3d NGWF initial guess, which results from poorer convergence characteristics when those functions are initialised with excessive localization.

Turning next to the LDA-appropriate Hubbard U and Hund’s J parameters calculated for TiO₂-anatase using the same method with a neutral Ti 3d subspace definition, shown in Table II, we note a remarkable degree of similarity with the TiO₂-rutile values. In fact, the differences are within the noise of the linear-response method, and this reflects the similar LDA charge states (to well within 1% for both the Ti 3d and O 2p DFT+ U subspaces) and coordination chemistry in the two structures.

A. The first-principles band gap of pristine TiO₂-rutile

As a generalized Kohn-Sham theory with an differentiable density-matrix dependence, in same way that hybrid functionals are⁵⁰, the Kohn-Sham gap of DFT+ U (or DFT+ U + J) includes an explicit derivative discontinuity. The relationship between the Kohn-Sham gap and the fundamental gap is thereby not only assured in principle, but the derivative discontinuity gives, in practice, the opportunity for direct comparability to the experi-

LDA anatase	Ti	O
U	3.57	8.56
J	0.29	0.91
$U_{\text{eff}} = U - J$	3.28	7.66
$U_{\text{full}} = U - 2J$	3.00	6.75

TABLE II. First-principles LDA-appropriate Hubbard U and Hund's J parameters calculated using the minimum-tracking linear-response method^{49,70}, both for the Ti $3d$ and O $2p$ subspaces of TiO₂-anatase. Only the neutral pseudo-atomic solver configuration Ti⁰ is used here. Shown also are the effective Hubbard U parameter of the Dudarev model (U_{eff}) and that which reproduces the DFT+ U + J functional (with minority term IV) for closed-shell systems (U_{full}).

mental insulating gap. Shown in Table III is the band gap of TiO₂-rutile calculated using LDA and first-principles DFT+ U , DFT+ U_{eff} , DFT+ U_{full} with different α values, and explicit DFT+ U + J (minority spin term (IV) neglected), both when applied only to the Ti $3d$ sub-shell and when applied also to the O $2p$ sub-shell.

Experimental, first-principles, semi-empirical hybrid, GW results, and several previous DFT+ U results from the literature are also shown in Table III, for comparison. The experimental direct gap quoted^{12,13} is based on absorption, photoluminescence, and resonant-Raman scattering data, and is expected to be very reliable due to the relatively small exciton binding and phonon coupling effects in rutile¹¹, and moreover in light of its good agreement with available inverse photoemission data⁷⁴.

The LDA yields a Kohn-Sham band gap of 1.96 eV, much lower than the experimental band gap of 3.03 eV, as expected given its absence of a derivative discontinuity. Regardless of the Hund's J incorporation scheme used, and as is generally attested in the literature on calculations with $J = 0$ eV, first-principles DFT+ U applied to Ti $3d$ states only performs poorly and here predicts a band gap of 2.17–2.24 eV. The inadequacy of the conventional DFT+ U subspace definition can be explained by comparing the very different valence and the conduction band edges characters seen in all of the local density of states plots shown in Fig. 1, and additionally motivated by recalling the very similar degree of spatial localization of Ti $3d$ and O $2p$ atomic orbitals (see Fig. 3). The valence (conduction) band edge is left almost unaffected by applying the Hubbard correction only to the Ti $3d$ (O $2p$) sub-shell, regardless of any reasonable Hubbard U parameter (hence, unreasonable values have been tested in the prior literature). In qualitative agreement with that, we observe that the impact of the method on the band-gap increases substantially as soon as correction is also applied to both subshells, within DFT+ $U^{d,p}$ (as we show in detail in Table III).

Focusing on our own first-principles DFT+ $U^{d,p}$ results and comparing with experiment, we find that when the correction for energy-magnetization curvature is ne-

TiO ₂ -rutile E_{gap}		
DFT (LDA)	1.96	
	U^d	$U^{d,p}$
DFT+ U	2.24	3.59
DFT+ $U_{\text{eff}} = U - J$	2.21	3.38
DFT+ $U_{\text{full}} = U - 2J, \alpha = -J/2$	2.17	3.32
DFT+ $U_{\text{full}} = U - 2J$	2.18	3.18
DFT+ $U_{\text{full}} = U - 2J, \alpha = J/2$	2.20	3.04
DFT+ U + J (no minority spin term)	2.20	3.04
Experiment ^{12,13}		3.03
LDA ⁴⁸		1.79
PBE ¹⁹		1.88
PBE ⁷⁵		1.86
PBE ⁷⁶		1.77
TB-mBJ ⁷⁷		2.60
SCAN ⁷⁸		2.23
HSE06 ⁷⁹		3.3
HSE06 ¹⁹		3.39
HSE06 ($\alpha = 0.2$) ⁷⁶		3.05
sX Hybrid ⁷⁵		3.1
LDA+G ₀ W ₀ ¹⁸		3.34
PBE+G ₀ W ₀ ¹⁹		3.46
HSE+G ₀ W ₀ ¹⁹		3.73
DFT+ U ($U=7.5$ eV) ⁸⁰		2.83
DFT+ U ($U=10$ eV) ⁸¹		2.97
DFT+ U^d ($U = 3.25$ eV) ⁸²		2.01
DFT+ $U^{d,p}$ ($U^d = 3.25$ eV, $U^p = 10.65$ eV) ⁸²		3.67
DFT+ $U^{d,p}$ ($U^d = 3.25$ eV, $U^p = 5.0$ eV) ⁸²		2.69
DFT+ $U^{d,p}$ ($U^d = 0.15$ eV, $U^p = 7.34$ eV) ⁸³		2.83

TABLE III. The fundamental band gap (in eV) of TiO₂-rutile calculated within DFT(LDA), DFT+ U with Hund's J neglected, when treated within the Dudarev model (U_{eff}), and when treated in a manner which fully reproduces DFT+ U + J using only DFT+ U code for closed-shell systems (U_{full}), both when treated with ($\alpha = -J/2$) and without ($\alpha = J/2$) its minority-spin (term IV). DFT+ U^d and DFT+ $U^{d,p}$ results are separately shown, using parameters calculated from first principles using the minimum-tracking linear-response method, using only the neutral pseudo-atomic solver configuration Ti⁰. Prior experimental, first-principles local, semi-local, meta-generalized-gradient, and semi-empirical hybrid functional; perturbative G₀W₀; empirical, first-principles SCF linear-response (Ref. 82), and ACBN0 (Ref. 83) DFT+ U values are provided for convenient comparison. Our central results are highlighted in bold.

glected (letting $J = 0$ eV), the band gap is overestimated by ~ 0.56 eV with respect to the experimental gap. The important point here is that, even though the system harbors no magnetism in its ground-state, this does not imply that the error in the approximate energy functional related to the magnetic degree of freedom vanishes. When including this effect only in the like-spin term, (using Dudarev's $U_{\text{eff}} = U - J$) this overestimation reduces to ~ 0.35 eV, and when also applying the unlike-spin term (using $U_{\text{full}} = U - 2J$ and $\alpha = -J/2$, which is equivalent to DFT+ $U+J$ including its standard minority spin term (IV), for closed-shell systems such this one), the overestimation reduces further to ~ 0.29 eV.

However, when we apply DFT+ $U+J$ in its simplest form, i.e., neglecting the minority spin term (IV) of Eq. (2) (in practice using $U_{\text{full}} = U - 2J$ and $\alpha = J/2$), the gap underestimation vanishes to within the expected error in the experiment (using the zero-temperature extrapolation of the direct fundamental gap provided in Ref. 12) and the theoretical methodology. We note that the zero-point phonon correction is held to be very small in rutile, unlike in anatase. As shown in Table III, we also carried out DFT+ $U+J$ calculations using explicit + J code, with the same results to a high precision, as predicted. We note, in passing, that the deduction in the calculated gap due to the omission of the minority spin term, of ~ 0.29 eV, is very close to $(J^p - J^d)/2 \sim 0.31$ eV, as might be predicted by considering the different characters of the band edges and the change in the potentials acting upon them.

These fundamental gap changes are reflected in the local density of states (LDOS) plots shown in Fig. 1. Here, we see the successive effects of first turning on + $U^{d,p}$ correction, and then by moderating it using J per Dudarev's $U_{\text{eff}} = U - J$ prescription, which mostly brings the valence band back up in energy in this case. Moving ultimately to DFT+ $U_{\text{full}}^{d,p}$, $\alpha = J/2$ (which means $\alpha^d = J^d/2$, etc., and which gives identical results to DFT+ $U^{d,p}+J^{d,p}$ by construction), we see a further closing of the gap and upward shift both in the valence and conduction bands. Interestingly, we obtain an extremely similar valence-band DoS from the Dudarev prescription and DFT+ $U_{\text{full}}^{d,p}$, $\alpha = -J/2$, i.e. DFT+ $U^{d,p}+J^{d,p}$ with the minority spin term intact. This reflects the almost-complete cancellation of the potentials due to terms (III) and (IV) in Eq. (2), for a subspace near full occupancy.

B. The first-principles band gap of pristine TiO₂-anatase

A similar procedure was followed for pristine TiO₂-anatase as that which we have outlined for TiO₂-rutile, except that only the neutral atomic configuration of Ti was used in the pseudo-atomic solver, in view of our previously discussed findings. As reflected in the calculated U and J parameters of Tables I and II, the electronic structures of the two polymorphs are rather sim-

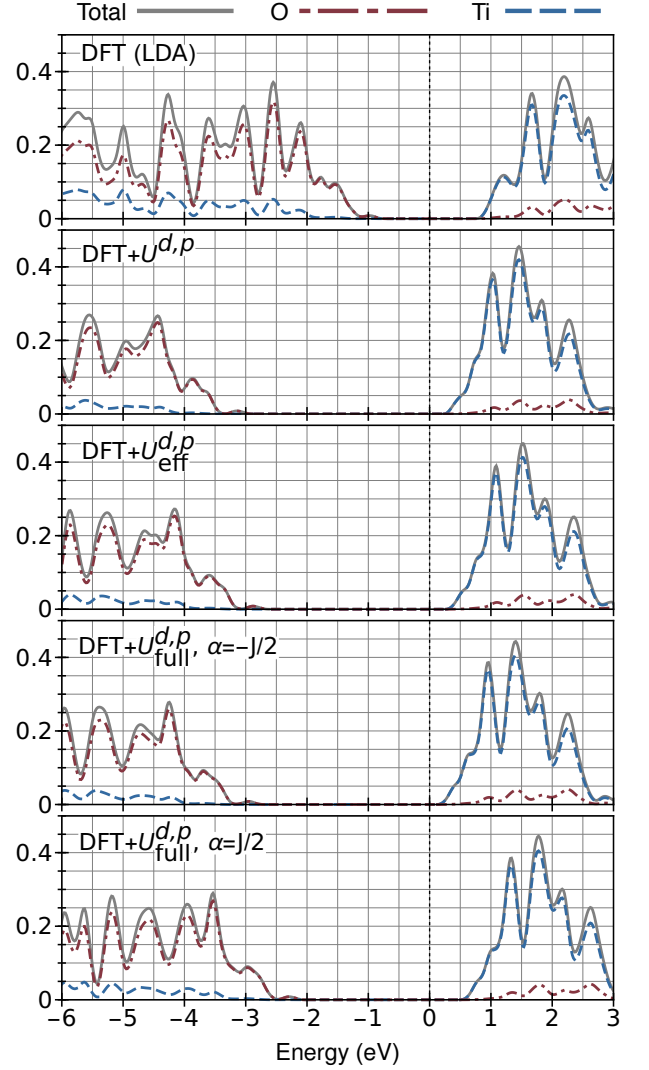


FIG. 1. The total and local generalized Kohn-Sham density of states (LDOS) of pristine TiO₂-rutile calculated within DFT(LDA), DFT+ U with Hund's J neglected, when treated within the Dudarev model (U_{eff}), and when treated in a manner which fully reproduces DFT+ $U+J$ using only DFT+ U code for closed-shell systems (U_{full}), both when treated with ($\alpha = -J/2$) and without ($\alpha = J/2$) its minority-spin (term IV). The spectrum is partitioned on a per-species basis using Mulliken analysis based on the variationally optimized NG-WFs. DFT+ $U^{d,p}$ results only are shown, using parameters calculated from first principles using the minimum-tracking linear-response method, using only the Ti⁰ pseudo-atomic solver configuration, and a Gaussian broadening of 0.1 eV. In order to show the separate effects of the corrective functionals tested on the valence and conduction bands, each panel uses the mid-gap energy of the DFT(LDA) calculation for 0 eV.

ilar, and again the valence (conduction) band edge is dominated by O 2p (Ti 3d) character in TiO₂-anatase, necessitating DFT+ $U^{d,p}$ for successful gap correction. Shown in Table IV is the fundamental band gap of TiO₂-anatase calculated using LDA and first-principles DFT+ U , DFT+ U_{eff} , DFT+ U_{full} , and DFT+ $U+J$ (mi-

TiO ₂ -anatase E_{gap}		
DFT (LDA)	2.21	
	$+U^d$	$+U^{d,p}$
DFT+ U	2.51	4.13
DFT+ $U_{\text{eff}} = U - J$	2.48	3.88
DFT+ $U_{\text{full}} = U - 2J, \alpha = -J/2$	2.41	3.81
DFT+ $U_{\text{full}} = U - 2J$	2.45	3.65
DFT+ $U_{\text{full}} = U - 2J, \alpha = J/2$	2.49	3.50
DFT+ $U+J$ (no minority spin term)	2.49	3.50
Experiment ¹¹	3.47	
PBE ¹⁹	1.94	
TB-mBJ ⁷⁷	3.01	
SCAN ⁷⁸	2.56	
HSE06 ^{19,79}	3.60	
LDA+G ₀ W ₀ ¹⁸	3.56	
PBE+G ₀ W ₀ ¹¹	3.61	
PBE+G ₀ W ₀ ¹⁹	3.73	
HSE+G ₀ W ₀ ¹⁹	4.05	
DFT+ U^d ($U=7.5$ eV) ⁸⁰	3.27	
DFT+ U^d ($U = 3.23$ eV) ⁸²	2.43	
DFT+ $U^{d,p}$ ($U^d = 3.23$ eV, $U^p = 10.59$ eV) ⁸²	4.24	
DFT+ $U^{d,p}$ ($U^d = 3.23$ eV, $U^p = 5.0$ eV) ⁸²	3.23	

TABLE IV. The band gap (in eV) of TiO₂-anatase calculated within DFT(LDA), DFT+ U with Hund's J neglected, when treated within the Dudarev model (U_{eff}), and when treated in a manner which fully reproduces DFT+ $U+J$ using only DFT+ U code for closed-shell systems (U_{full}), both when treated with ($\alpha = -J/2$) and without ($\alpha = J/2$) its minority-spin (term IV). DFT+ U^d and DFT+ $U^{d,p}$ results are separately shown, using parameters calculated from first principles using the minimum-tracking linear-response method, using only the neutral pseudo-atomic solver configuration Ti⁰. Prior experimental, first-principles local, semi-local, meta-generalized-gradient, and semi-empirical hybrid functional; perturbative G₀W₀; empirical and first-principles SCF linear-response DFT+ U (Ref. 82) values from the literature are provided for convenient comparison. Our central results are highlighted in bold.

nority spin term (IV) included, spin-averaged, and neglected), both when applied only to the Ti 3d sub-shell and when applied also to the O 2p sub-shell. The corresponding NGWF-partitioned Mulliken LDOS plots are shown in Fig. 2. We anticipate a slight overestimation in our calculated gap values for TiO₂-anatase, due to our necessarily finite effective sampling of the Brillouin zone. The band gap of anatase is of indirect character and, while our sampling is chosen to closely sample the LDA band edges, we cannot be guaranteed to precisely sample the valence band maximum (most studies hold the fundamental gap of rutile to be direct at Γ , on the

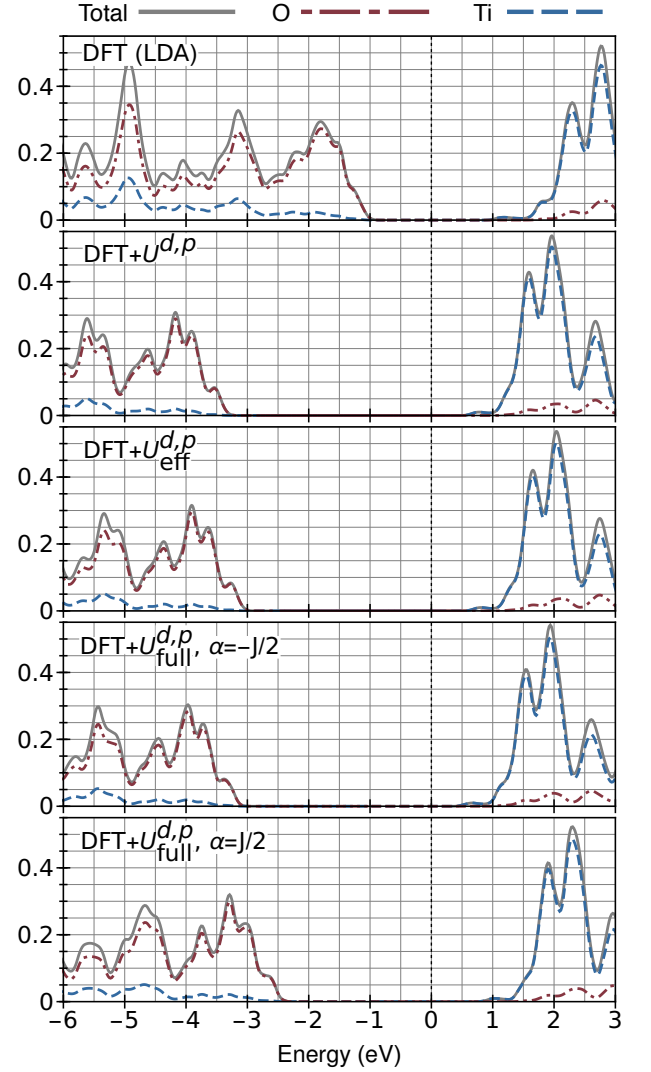


FIG. 2. The total and local generalized Kohn-Sham density of states (LDOS) of pristine TiO₂-anatase calculated within DFT(LDA), DFT+ U with Hund's J neglected, when treated within the Dudarev model (U_{eff}), and when treated in a manner which fully reproduces DFT+ $U+J$ using only DFT+ U code for closed-shell systems (U_{full}), both when treated with ($\alpha = -J/2$) and without ($\alpha = J/2$) its minority-spin (term IV). The spectrum is partitioned on a per-species basis using Mulliken analysis based on the variationally optimized NGWFs. DFT+ $U^{d,p}$ results only are shown, using parameters calculated from first principles using the minimum-tracking linear-response method, using only the Ti⁰ pseudo-atomic solver configuration, and a Gaussian broadening of 0.1 eV. In order to show the separate effects of the corrective functionals tested on the valence and conduction bands, each panel uses the mid-gap energy of the DFT(LDA) calculation for 0 eV.

other hand, which we do sample). Again, experimental, first-principles, semi-empirical hybrid, many-body perturbation theory, and several previous DFT+ U results from the literature are shown for comparison.

While anatase has been thoroughly studied using optical techniques⁸⁴, our focus here is on the fundamen-

tal electronic gap. For the latter, very little direct data is available, but fortunately there has recently been reported angle-resolved photoemission spectroscopy with n-type doping (to circumvent the need for inverse photoemission) in Ref. 11, strongly supported by temperature-dependent many-body perturbation theory calculations including electron-phonon coupling. The fundamental gap reported in the latter work is higher than that found elsewhere in older studies, and the reason is that, whereas the commonplace mis-identification between the optical and fundamental gap is not very significant for rutile (the exciton binding is ~ 4 meV), it is not at all reasonable for anatase, which is reported to exhibit relatively very large exciton binding ~ 0.18 eV effects in its low-energy optical spectra¹¹.

The LDA gives a Kohn-Sham band gap of 2.21 eV, substantially underestimating the experimental electronic gap of 3.47 eV. DFT+ U^d is ineffective at opening the gap as is in TiO₂-rutile, given the LDA-appropriate calculated first-principles U and J parameters. DFT+ $U^{d,p}$ opens the gap very efficiently and, closely mirroring what we found for TiO₂-rutile, both DFT+ U with J neglected and Dudarev's DFT+ U_{eff} cause the gap to be overestimated. Similarly, again, first-principles DFT+ $U+J$ including O $2p$ correction gives decent agreement with the experimental gap, overestimating it by 0.03 eV (0.34 eV) when the minority spin term is neglected (included). Interestingly, both the HSE06 and DFT+G₀W₀ approximations seem to better recover the anatase gap than the rutile one, based on the available literature. DFT+ U_{full} , $\alpha = J/2$ (which is to say, technically, first-principles DFT+ $U^{d,p}+J^{d,p}$ with the minority spin term neglected, which doesn't require an explicit Hund's J implementation for closed-shell systems) seems to be very competitive with respect to both methods as far as both the fundamental gap and computational complexity are concerned. The key ingredient for TiO₂ in this sort of method, aside from the established message that the O $2p$ subspace needs to be treated on the same footing as the Ti $3d$ one, is evidently to correct both for the usual charge-related (U) and spin-related (J) systematic errors in the approximate functional. Indeed, more generally it has been shown in Ref. 44, by using the 2×2 formalism to analyse the linear-response approach for Hubbard U parameter calculation, that the non-neglect of Hund's J is advisable even on abstract consistency grounds.

IV. CONCLUSIONS

We have shown that the DFT+ $U+J$ functional developed in Ref. 43, in combination with the first-principles procedure for calculating U and J parameters developed in Ref. 44, yields fundamental gaps that are in very close agreement with the most sophisticated available zero-temperature-approaching experimental findings for TiO₂. The residual errors, 0.01 eV for rutile and 0.03 eV for anatase, are within the anticipated errors due to fac-

tors such as neglected zero-point phonon motion and relativistic effects, the pseudopotential approximation, imperfect Brillouin zone sampling (more relevant for anatase), and various sources of experimental uncertainty. Interestingly, the method performs better than both hybrid functionals and perturbative G₀W₀ for the fundamental gap, while retaining a semi-local DFT-like level of computational cost (even linear-scaling⁷⁰, algorithmically, though we don't exploit that here).

An important and surprising finding of this work, which we go on to discuss in Appendix B, is that, contrary to our expectation, the first-principles calculation of U and J for TiO₂-rutile acts to reinforce the numerically-significant arbitrariness⁸⁵ of DFT+ U with respect to the (too often unstated) choice of localized orbitals defining the subspaces targeted for correction. The good news here is that it is the default, neutrally-charged, isolated atomic configuration that yields the accurate gaps. In our experience to date, the introduction of chemical intuition when defining atomic solver charge states for DFT+ U projector construction yields worsened results together with worsened convergence behaviour.

We judge that our results are, overall, very encouraging for the continued, very widespread use of DFT+ U and its extensions for studying TiO₂, and that they serve as a counter-example to the concept that such methods are fundamentally limited in their applicability to high-spin systems. It remains for a future study to establish whether TiO₂ is a special case for the Ref. 43 and Ref. 44 combination, or whether it is as successful for oxides, particularly closed-shell oxides, more generally. What has hampered closed-shell applications to date, as highlighted in Ref. 86, have been available Hubbard U values, calculated or otherwise, that are too high for practical use. Our results demonstrate that Hund's J , which is subtracted from U once in the Dudarev formalism, and effectively *twice* in DFT+ $U+J$ for closed-shell systems, yielding $U_{\text{full}} = U - 2J$, may be the key ingredient to moderating the U . The first-principles U values in common circulation for Ti $3d$ orbitals in TiO₂, in the range of approximately 3 – 4 eV depending on the projector choice, are perhaps fine after all. Meanwhile, our directly calculated, relatively high-seeming-at-first U values for O $2p$ orbitals in TiO₂ (which are more localised than Ti $3d$ ones, see the plot in Fig. 3) sit among the few previously reported calculated values for TiO₂ in the literature^{83,87}.

Our results are consistent with the prescriptions detailed in Ref. 43 and Ref. 44, for the use and calculation of U and J parameters, respectively, being correct. The contribution of the explicit unlike-spin J correction (term (III) in Eq. (2)) to the potential subspace matrix elements for spin σ , is given by $V_{mm'}^{J\sigma} = Jn_{mm'}^{\bar{\sigma}}$. It seems that this is a very good approximation, given that there are J parameters involved for two different subspace types and the net result is very accurate as far as the gap is concerned. Our results strongly support the conclusions of Ref. 43 that the minority spin term (IV) of Eq. (2), which arises only due to the double-counting correction

of a unlike-spin interaction that unlikely to be well described in the underlying functional in the first place, should be neglected. Equivalently, they support the conclusion that the fully localized limit double-counting term of Refs. 88 and 89 is sufficient at this level of theory, at least as far as the potential is concerned. The DFT+ $U+J$ gap is just one aspect of the potential, of course, and its correctness cannot be used to judge whether the double-counting in the total energy is correct, for example. In previous works, we have pointed out cases where the standard DFT+ U potential fails due to non-satisfaction of Koopmans' condition⁹⁰, or due to inadequate projection onto the states adjacent to the band edges⁹¹, neither of which effects are expected to be alleviated particularly by the incorporation of Hund's J .

On a similar cautionary note, it is worth emphasizing that our first-principle calculations of U and J in TiO₂ were made simpler by the vanishing occupancy-magnetization coupling in closed-shell systems, by which we mean that $d(n^\uparrow + n^\downarrow)/d\beta = 0 = d(n^\uparrow - n^\downarrow)/d\alpha$. In this case, the elegant formulae of Eq. (8) become unambiguous with respect to the spin-polarization of the perturbing potential. In our current view, these two formulae are essentially the correct ones for U and J , neglecting self-consistency over parameters. As a result, without approximation and very conveniently, we were able to perturb one spin only and obtain U and J simultaneously. A disadvantage of this decoupling, however, is that we cannot judge on the basis of the present calculations between the merits of the “scaled 2×2 ” and “simple 2×2 ” procedures of Ref. 44, since they become identical. Overall, there is without doubt much further work to be done on developing self-contained corrective techniques such as first-principles DFT+ $U+J$ for approximate density-functional theory, which side-step the evolution of increasingly costly closed-form functionals. Meanwhile, our results here may prove to significantly lower the computational barrier to simulating accurate spectral quantities in large, possibly defect-containing or disordered super-cells of TiO₂.

V. ACKNOWLEDGEMENTS

We wish to thank Glenn Moynihan, Edward Lin-scott, Gilberto Teobaldi, and Harald Oberhofer for helpful discussions. We acknowledge the support of Trinity College Dublin School of Physics, Science Foundation Ireland (SFI) through The Advanced Materials and Bioengineering Research Centre (AMBER, grant 12/RC/2278 and 12/RC/2278.P2), and the European Regional Development Fund (ERDF). We also acknowledge the DJEI/DES/SFI/HEA Irish Centre for High-End Computing (ICHEC) for the provision of computational facilities and support. We further acknowledge Trinity Centre for High Performance Computing and Science Foundation Ireland, for the maintenance and funding, respectively, of the Boyle (Cuimhne upgrade) cluster on

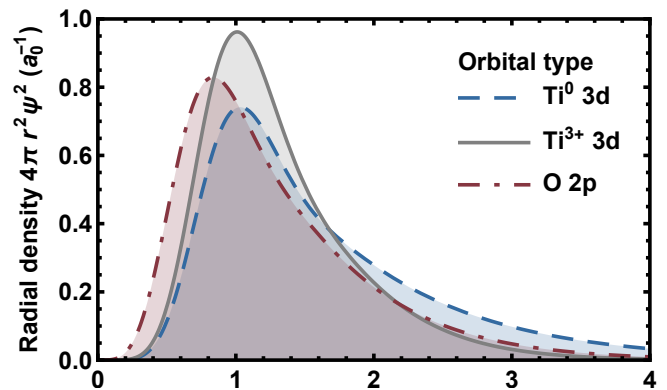


FIG. 3. The radial probability distributions of the three pseudo-orbital types used to define DFT+ $U(+J)$ subspaces in this work, as defined in the main text. The oxygen $2p$ subspaces are more localised than their titanium $3d$ counterparts, and thus are reasonable candidates for correction testing. The Ti pseudo-atomic solver charge state significantly affects the localization of the $3d$ orbitals, and the resulting gaps.

which further calculations were performed.

Appendix A: DFT+ U on $2p$ and $3d$ orbitals: DFT+ $U^{d,p}$

In principle, SIE is harboured by all subshells and cannot be partitioned out between them, however, it is commonly more dominant in $3d$ subshells due to their spatially localized nature. Hence, in titanium-comprising systems, the Hubbard correction in DFT+ U is conventionally applied to the $3d$ subshell only. The Hubbard U parameters used for the $3d$ orbitals of Ti atom have ranged over $\sim 2.5 - 10$ eV⁹², and have most commonly been determined by tuning to some observed quantity^{87,93–98}. Even when overlooking our serious concerns regarding the robustness and conceptual validity of U value calibration to observable quantities, particularly when those are not ground-state observables, a practical problem arises for DFT+ U due to the location of Ti on the extreme left of the transition-metal block. It is well known that Hubbard U correction to the $3d$ -orbitals alone is not very effective for opening the band gap of TiO₂, which saturates even with unreasonably large U values, as the dominant $2p$ -states at the valence band-edge remain barely affected. Moreover, when actually plotted, as they are in Fig. 3 the $2p$ pseudo-orbitals of O atoms are rather *more* localized than their Ti $3d$ counterparts, and so it is not at all unreasonable, quite the contrary, to calculate (or at least tune, where calculation is not possible) Hubbard U and even Hund's J parameters for O $2p$. Indeed, it has been demonstrated in several prior works that applying the Hubbard U correction simultaneously on the $3d$ orbitals of Ti and the $2p$ orbitals of O atoms, symbolically giving DFT+ $U^{d,p}$, readily addresses the aforementioned gap saturation problem

and provides a more accurate description of the band structure around the Fermi level^{45–48}.

Appendix B: The effects on the density of states of the choice of pseudo-atomic solver configuration for generating the Ti 3d DFT+ U subspace

TiO ₂ -rutile E_{gap}				
Subspace definition	Ti ⁰		Ti ³⁺	
DFT(LDA)	1.96		1.96	
	+ U^d	+ $U^{d,p}$	+ U^d	+ $U^{d,p}$
U	2.24	3.59	2.69	4.20
$U_{\text{eff}} = U - J$	2.21	3.38	2.63	3.94
$U_{\text{full}} = U - 2J, \alpha = -J/2$	2.17	3.32	2.52	3.81
$U_{\text{full}} = U - 2J$ from Ti ⁰	2.18	3.18	2.31	3.33
$U_{\text{full}} = U - 2J$ from Ti ³⁺	2.38	3.46	2.57	3.69
$U_{\text{full}} = U - 2J, \alpha = J/2$	2.20	3.04	2.62	3.58
$U+J$ (no minority spin term)	2.20	3.04	2.64	3.58

TABLE V. This table highlights the arbitrariness of DFT+ U with respect to the targeted subspace choice, which is not compensated for in this system by first-principles calculation of the U and J parameters. Shown is the band gap (in eV) of TiO₂-rutile calculated within DFT(LDA), DFT+ U with Hund’s J neglected, when treated within the Dudarev model (U_{eff}), and when treated in a manner which fully reproduces DFT+ $U+J$ using only DFT+ U code (U_{full}). DFT+ U^d and DFT+ $U^{d,p}$ results are separately shown, and these depend on the pseudo-atomic solver configuration (neutral or 3+) used to define the targeted Ti 3d subspace, together with the corresponding subspace-dependent U and J parameters. For the intermediate case of U_{full} with $\alpha = 0$, i.e., DFT+ $U+J$ with its minority term split over the two spins, we show the effect on the gap of separately changing the subspace used to calculate the parameters, and the subspace used to apply the parameters, revealing that these effects combine to reinforce, not to cancel, the subspace-dependence in this system. The gaps from “mismatched” calculations, with parameters from the other subspace type, are shown in bold.

For the specific case of rutile, we investigate in detail here the effect of varying the charge configuration for Ti used in the pseudo-atomic solver⁷², which constructs the set of the pseudo-atomic orbitals defining the 3d subspace of Ti. The neutral configuration is perhaps a natural choice, giving the relatively smooth, diffuse subspace shown in Fig. 3. This results in less pressure on the plane-wave convergence and, more importantly, it does not rely on any prior chemical intuition. We also investigated the 3+ atomic charge configuration, as a slightly more “informed” spatially localized subspace test case. Given the LDA-appropriate U and J parameters calculated for each of the two subspace types and presented in Table I, we performed the matching DFT+ U ,

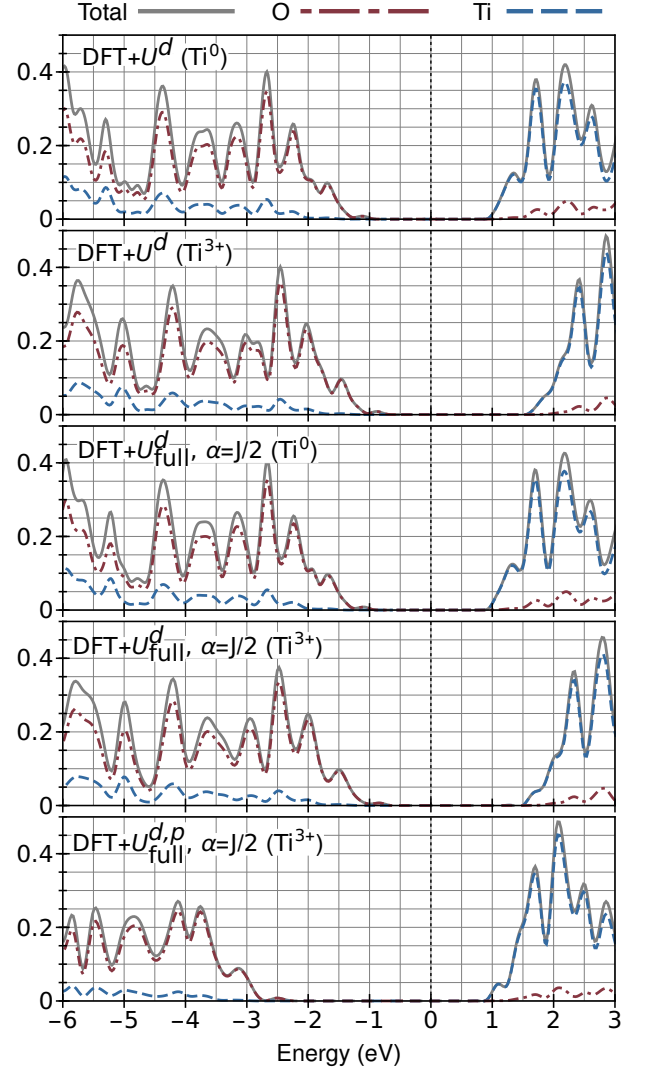


FIG. 4. The total and local generalized Kohn-Sham density of states (LDOS) of pristine TiO₂-rutile calculated within DFT+ U^d , separately for Ti⁰ and Ti³⁺ subspace definitions, within DFT+ U^d+J^d for the same two subspace definitions, and finally within DFT+ $U^{d,p}+J^{d,p}$ for the Ti³⁺ definition. The spectrum is partitioned on a per-species basis using Mulliken analysis based on the variationally optimized NGWFs. Parameters were calculated from first principles using the minimum-tracking linear-response method, and a Gaussian broadening of 0.1 eV was used. Each panel uses the mid-gap energy of the DFT+ U^d (Ti⁰) calculation for 0 eV.

DFT+ U_{eff} , and DFT+ $U+J$ band-gap calculations, both within DFT+ U^d and DFT+ $U^{d,p}$. We also performed the “cross” calculations in the case of $\alpha = 0$, i.e., where we used the 3+ subspace parameters for correcting the neutral subspace, and vice-versa, in order to illustrate the separate effects of over-localizing the projectors.

The results of these tests are shown in Table V. We find that first-principles calculation of the Hubbard U and Hund’s J parameters does not compensate for the arbitrariness of the subspace choice, for Ti 3d. Instead,

it reinforces this arbitrariness as far as the fundamental gap is concerned in this system. Table V reveals that this trend holds irrespective of whether correction is also applied to O $2p$ orbitals, denoted DFT+ $U^{d,p}$, or indeed whether we are using DFT+ U , DFT+ U_{eff} , or DFT+ U_{full} . As previously discussed, the increase in spatial localization of the $3d$ subspace, when we move from a neutral to a $3+$ configuration, increases the corresponding calculated U and J parameters. This, of course, increases the predicted gap, when those parameters are applied to either subspace type. Moreover, Table V demonstrates that, for either fixed set of parameters, the increase in subspace localization also tends to open the gap, in this system, in fact by roughly the same amount. The net increase in the gap in going from the neutral to $3+$ subspace densities shown in Fig. 3, with corresponding first-principles parameters, is thus approximately due, half-and-half, to the increase in parameters and increase in localization.

On the basis of these results, we can envisage that both the first-principles LDA-appropriate U and J parameters, and the fundamental gap for a fixed reasonable set of parameters, will attain maxima for some reasonable (though not generally the same) value of the pseudo-atomic configuration charge. A tentative step towards plotting observables as functions of a DFT+ U subspace localization quantifier was presented in Ref. 85.

More recently, the projector dependence of DFT+ U results on rutile TiO_2 has previously been demonstrated at fixed U values in Ref. 99. We do not necessarily expect that the projector arbitrariness reinforcement effect will arise transition-metal oxides generally, particularly since projector arbitrariness cancellation has previously been observed in molecular FeO^+ using a self-consistently evaluated Hubbard U parameter¹⁰⁰. This issue in DFT+ U clearly warrants further investigation on diverse systems using various approaches, such as parameter^{49,68} or projector^{85,101} self-consistency. Pragmatically, we have found, in our minimum-tracking linear-response calculations to date, that using the simplest, neutral pseudo-atomic configuration for constructing the DFT+ U projections works well relative to more localised charged configurations. This is irrespective of the pseudopotential generator reference state, which is a somewhat different, technical matter related the transferability in norm-conserving pseudopotentials. We note, in passing, that there is a small discrepancy in the gap from Ti^{3+} -only subspace explicit DFT+ $U+J$ and the corresponding unmodified-DFT+ U -code equivalent form with $\alpha = J/2$, reflecting that calculations with excessively localised subspaces are typically less numerically stable, aside from giving less favorable results.

- ¹ A. Salvador, M. Pascual-Martí, J. Adell, A. Requeñi, and J. March, Analytical methodologies for atomic spectrometric determination of metallic oxides in uv sunscreen creams, *Journal of Pharmaceutical and Biomedical Analysis* **22**, 301 (2000).
- ² J. H. Braun, A. Baidins, and R. E. Marganski, TiO_2 pigment technology: A review, *Progress in Organic Coatings* **20**, 105 (1992).
- ³ F. J. Maile, G. Pfaff, and P. Reynders, Effect pigments - past, present and future, *Progress in Organic Coatings* **54**, 150 (2005).
- ⁴ A. Fujishima and H. Kenichi, Electrochemical photolysis of water at a semiconductor electrode, *Nature* **238**, 37 EP (1972).
- ⁵ K. Hashimoto, H. Irie, and A. Fujishima, TiO_2 photocatalysis: A historical overview and future prospects, *Japanese Journal of Applied Physics* **44**, 8269 (2005).
- ⁶ X. Chen and S. S. Mao, Titanium dioxide nanomaterials synthesis, properties, modifications, and applications, *Chemical Reviews* **107**, 2891 (2007).
- ⁷ M. Pelaez, N. T. Nolan, S. C. Pillai, M. K. Seery, P. Falaras, A. G. Kontos, P. S. Dunlop, J. W. Hamilton, J. Byrne, K. O'Shea, M. H. Entezari, and D. D. Dionysiou, A review on the visible light active titanium dioxide photocatalysts for environmental applications, *Applied Catalysis B: Environmental* **125**, 331 (2012).
- ⁸ D. Reyes-Coronado, G. Rodríguez-Gattorno, M. E. Espinosa-Pesqueira, C. Cab, R. de Coss, and G. Oskam, Phase-pure TiO_2 nanoparticles: Anatase, brookite and rutile, *Nanotechnology* **19**, 145605 (2008).
- ⁹ D. Dambournet, I. Belharouak, and K. Amine, Tailored preparation methods of TiO_2 anatase, rutile, brookite: Mechanism of formation and electrochemical properties, *Chemistry of Materials* **22**, 1173 (2010).
- ¹⁰ J. Pascual, J. Camassel, and H. Mathieu, Resolved quadrupolar transition in TiO_2 , *Phys. Rev. Lett.* **39**, 1490 (1977).
- ¹¹ E. Baldini, L. Chiodo, A. Dominguez, M. Palummo, S. Moser, M. Yazdi-Rizi, G. Auböck, B. P. P. Mallett, H. Berger, A. Magrez, C. Bernhard, M. Grioni, A. Rubio, and M. Chergui, Strongly bound excitons in anatase TiO_2 single crystals and nanoparticles, *Nature Communications* **8**, 13 (2017).
- ¹² J. Pascual, J. Camassel, and H. Mathieu, Fine structure in the intrinsic absorption edge of TiO_2 , *Phys. Rev. B* **18**, 5606 (1978).
- ¹³ A. Amtout and R. Leonelli, Optical properties of rutile near its fundamental band gap, *Phys. Rev. B* **51**, 6842 (1995).
- ¹⁴ H. Tang, F. Lévy, H. Berger, and P. E. Schmid, Urbach tail of anatase TiO_2 , *Phys. Rev. B* **52**, 7771 (1995).
- ¹⁵ W. Mackrodt, E.-A. Simson, and N. Harrison, An ab initio hartree-fock study of the electron-excess gap states in oxygen-deficient rutile TiO_2 , *Surface Science* **384**, 192 (1997).
- ¹⁶ S.-D. Mo and W. Y. Ching, Electronic and optical properties of three phases of titanium dioxide: Rutile, anatase, and brookite, *Phys. Rev. B* **51**, 13023 (1995).
- ¹⁷ Y.-f. Zhang, W. Lin, Y. Li, K.-n. Ding, and J.-q. Li, A theoretical study on the electronic structures of TiO_2 : effect of hartreefock exchange, *The Journal of Physical Chemistry B* **109**, 19270 (2005), pMID: 16853489.

- ¹⁸ W. Kang and M. S. Hybertsen, Quasiparticle and optical properties of rutile and anatase TiO₂, *Phys. Rev. B* **82**, 085203 (2010).
- ¹⁹ M. Landmann, E. Rauls, and W. G. Schmidt, The electronic structure and optical response of rutile, anatase and brookite TiO₂, *Journal of Physics: Condensed Matter* **24**, 195503 (2012).
- ²⁰ M. O. Atambo, D. Varsano, A. Ferretti, S. S. Ataei, M. J. Caldas, E. Molinari, and A. Selloni, Electronic and optical properties of doped TiO₂ by many-body perturbation theory, *Phys. Rev. Materials* **3**, 045401 (2019).
- ²¹ P. Hohenberg and W. Kohn, Inhomogeneous electron gas, *Phys. Rev.* **136**, B864 (1964).
- ²² W. Kohn and L. J. Sham, Self-consistent equations including exchange and correlation effects, *Phys. Rev.* **140**, A1133 (1965).
- ²³ D. C. Langreth and J. P. Perdew, Theory of nonuniform electronic systems. i. analysis of the gradient approximation and a generalization that works, *Phys. Rev. B* **21**, 5469 (1980).
- ²⁴ J. P. Perdew, Density-functional approximation for the correlation energy of the inhomogeneous electron gas, *Phys. Rev. B* **33**, 8822 (1986).
- ²⁵ J. P. Perdew, J. A. Chevary, S. H. Vosko, K. A. Jackson, M. R. Pederson, D. J. Singh, and C. Fiolhais, Atoms, molecules, solids, and surfaces: Applications of the generalized gradient approximation for exchange and correlation, *Phys. Rev. B* **46**, 6671 (1992).
- ²⁶ J. C. A. Prentice, J. Aarons, J. C. Womack, A. E. A. Allen, L. Andrinopoulos, L. Anton, R. A. Bell, A. Bhandari, G. A. Bramley, R. J. Charlton, R. J. Clements, D. J. Cole, G. A. Constantinescu, F. Corsetti, S. M.-M. Dubois, K. K. B. Duff, J. M. Escartín, A. Greco, Q. Hill, L. P. Lee, E. Linscott, D. D. O'Regan, M. J. S. Phipps, L. E. Ratcliff, A. R. Serrano, E. W. Tait, G. Teobaldi, V. Vitale, N. Yeung, T. J. Zuehlsdorff, J. Dziedzic, P. D. Haynes, N. D. M. Hine, A. A. Mostofi, M. C. Payne, and C.-K. Skylaris, The onetep linear-scaling density functional theory program, *The Journal of Chemical Physics* **152**, 174111 (2020).
- ²⁷ C.-K. Skylaris, P. D. Haynes, A. A. Mostofi, and M. C. Payne, Introducing onetep: Linear-scaling density functional simulations on parallel computers, *The Journal of Chemical Physics* **122**, 084119 (2005).
- ²⁸ P. D. Haynes, C.-K. Skylaris, A. A. Mostofi, and M. C. Payne, Onetep: Linear-scaling density-functional theory with local orbitals and plane waves, *physica status solidi (b)* **243**, 2489 (2006).
- ²⁹ L. E. Ratcliff, N. D. M. Hine, and P. D. Haynes, Calculating optical absorption spectra for large systems using linear-scaling density functional theory, *Phys. Rev. B* **84**, 165131 (2011).
- ³⁰ V. I. Anisimov, A. I. Poteryaev, M. A. Korotin, A. O. Anokhin, and G. Kotliar, First-principles calculations of the electronic structure and spectra of strongly correlated systems: dynamical mean-field theory, *Journal of Physics: Condensed Matter* **9**, 7359 (1997).
- ³¹ G. Pacchioni, Modeling doped and defective oxides in catalysis with density functional theory methods: Room for improvements, *The Journal of Chemical Physics* **128**, 182505 (2008).
- ³² M. V. Ganduglia-Pirovano, A. Hofmann, and J. Sauer, Oxygen vacancies in transition metal and rare earth oxides: Current state of understanding and remaining challenges, *Surface Science Reports* **62**, 219 (2007).
- ³³ S. L. Dudarev, G. A. Botton, S. Y. Savrasov, C. J. Humphreys, and A. P. Sutton, Electron-energy-loss spectra and the structural stability of nickel oxide: An LSDA+U study, *Phys. Rev. B* **57**, 1505 (1998).
- ³⁴ V. I. Anisimov and O. Gunnarsson, Density-functional calculation of effective coulomb interactions in metals, *Phys. Rev. B* **43**, 7570 (1991).
- ³⁵ V. I. Anisimov, J. Zaanen, and O. K. Andersen, Band theory and mott insulators: Hubbard *u* instead of stoner *i*, *Phys. Rev. B* **44**, 943 (1991).
- ³⁶ V. I. Anisimov, I. V. Solovyev, M. A. Korotin, M. T. Czyżyk, and G. A. Sawatzky, Density-functional theory and NiO photoemission spectra, *Phys. Rev. B* **48**, 16929 (1993).
- ³⁷ I. V. Solovyev, P. H. Dederichs, and V. I. Anisimov, Corrected atomic limit in the local-density approximation and the electronic structure of d impurities in Rb, *Phys. Rev. B* **50**, 16861 (1994).
- ³⁸ A. I. Liechtenstein, V. I. Anisimov, and J. Zaanen, Density-functional theory and strong interactions: Orbital ordering in mott-hubbard insulators, *Phys. Rev. B* **52**, R5467 (1995).
- ³⁹ W. E. Pickett, S. C. Erwin, and E. C. Ethridge, Reformulation of the LDA+*U* method for a local-orbital basis, *Phys. Rev. B* **58**, 1201 (1998).
- ⁴⁰ M. Cococcioni and S. de Gironcoli, Linear response approach to the calculation of the effective interaction parameters in the LDA+*U* method, *Phys. Rev. B* **71**, 035105 (2005).
- ⁴¹ B. Himmetoglu, A. Floris, S. de Gironcoli, and M. Cococcioni, Hubbard-corrected DFT energy functionals: The LDA+*U* description of correlated systems, *International Journal of Quantum Chemistry* **114**, 14 (2014).
- ⁴² A. Seidl, A. Görling, P. Vogl, J. A. Majewski, and M. Levy, Generalized kohn-sham schemes and the band-gap problem, *Phys. Rev. B* **53**, 3764 (1996).
- ⁴³ B. Himmetoglu, R. M. Wentzcovitch, and M. Cococcioni, First-principles study of electronic and structural properties of CuO, *Phys. Rev. B* **84**, 115108 (2011).
- ⁴⁴ E. B. Linscott, D. J. Cole, M. C. Payne, and D. D. O'Regan, Role of spin in the calculation of Hubbard *u* and Hund's *j* parameters from first principles, *Phys. Rev. B* **98**, 235157 (2018).
- ⁴⁵ B. J. Morgan and G. W. Watson, Polaronic trapping of electrons and holes by native defects in anatase TiO₂, *Phys. Rev. B* **80**, 233102 (2009).
- ⁴⁶ M. Nolan and G. W. Watson, Hole localization in al doped silica: A DFT+*U* description, *The Journal of Chemical Physics* **125**, 144701 (2006).
- ⁴⁷ S. Lany and A. Zunger, Polaronic hole localization and multiple hole binding of acceptors in oxide wide-gap semiconductors, *Phys. Rev. B* **80**, 085202 (2009).
- ⁴⁸ S.-G. Park, B. Magyari-Köpe, and Y. Nishi, Electronic correlation effects in reduced rutile TiO₂ within the LDA + *u* method, *Phys. Rev. B* **82**, 115109 (2010).
- ⁴⁹ G. Moynihan, *A self-contained ground-state approach for the correction of self-interaction error in approximate density-functional theory*, Ph.D. thesis, School of Physics, Trinity College Dublin (2018).
- ⁵⁰ W. Yang, A. J. Cohen, and P. Mori-Sánchez, Derivative discontinuity, bandgap and lowest unoccupied molecular orbital in density functional theory, *The Journal of Chemical Physics* **136**, 204111 (2012).
- ⁵¹ A. J. Cohen, P. Mori-Sánchez, and W. Yang, Insights into

- current limitations of density-functional theory, *Science* **321**, 792 (2008).
- ⁵² R. Merkle, A. Savin, and H. Preuss, Singly ionized first-row dimers and hydrides calculated with the fully-numerical densityfunctional program numol, *The Journal of Chemical Physics* **97**, 9216 (1992).
 - ⁵³ A. Savin, On degeneracy, near-degeneracy and density functional theory (Louisiana State University, Baton Rouge, LA (United States), 1996).
 - ⁵⁴ J. P. Perdew and M. Levy, Comment on “significance of the highest occupied kohn-sham eigenvalue”, *Phys. Rev. B* **56**, 16021 (1997).
 - ⁵⁵ Y. Zhang and W. Yang, A challenge for density functionals: Self-interaction error increases for systems with a noninteger number of electrons, *The Journal of Chemical Physics* **109**, 2604 (1998).
 - ⁵⁶ J. P. Perdew and A. Zunger, Self-interaction correction to density-functional approximations for many-electron systems, *Phys. Rev. B* **23**, 5048 (1981).
 - ⁵⁷ P. Mori-Sánchez, A. J. Cohen, and W. Yang, Many-electron self-interaction error in approximate density functionals, *The Journal of Chemical Physics* **125**, 201102 (2006).
 - ⁵⁸ P. Mori-Sánchez, A. J. Cohen, and W. Yang, Self-interaction-free exchange-correlation functional for thermochemistry and kinetics, *The Journal of Chemical Physics* **124**, 091102 (2006).
 - ⁵⁹ O. A. Vydrov, G. E. Scuseria, J. P. Perdew, A. Ruzsinszky, and G. I. Csonka, Scaling down the perdew-zunger self-interaction correction in many-electron regions, *The Journal of Chemical Physics* **124**, 094108 (2006).
 - ⁶⁰ A. Ruzsinszky, J. P. Perdew, G. I. Csonka, O. A. Vydrov, and G. E. Scuseria, Spurious fractional charge on dissociated atoms: Pervasive and resilient self-interaction error of common density functionals, *The Journal of Chemical Physics* **125**, 194112 (2006).
 - ⁶¹ A. Ruzsinszky, J. P. Perdew, G. I. Csonka, O. A. Vydrov, and G. E. Scuseria, Density functionals that are one- and two- are not always many-electron self-interaction-free, as shown for $\text{h}2+$, $\text{he}2+$, $\text{lih}+$, and $\text{ne}2+$, *The Journal of Chemical Physics* **126**, 104102 (2007).
 - ⁶² A. J. Cohen, P. Mori-Sánchez, and W. Yang, Challenges for density functional theory, *Chemical Reviews* **112**, 289 (2012).
 - ⁶³ M. Mikami, S. Nakamura, O. Kitao, H. Arakawa, and X. Gonze, First-principles study of titanium dioxide: Rutile and anatase, *Japanese Journal of Applied Physics* **39**, L847 (2000).
 - ⁶⁴ S. L. Dudarev, A. I. Liechtenstein, M. R. Castell, G. A. D. Briggs, and A. P. Sutton, Surface states on NiO (100) and the origin of the contrast reversal in atomically resolved scanning tunneling microscope images, *Phys. Rev. B* **56**, 4900 (1997).
 - ⁶⁵ M. Samat, A. Ali, M. Taib, O. Hassan, and M. Yahya, Hubbard u calculations on optical properties of 3d transition metal oxide to2, *Results in Physics* **6**, 891 (2016).
 - ⁶⁶ See Supplemental Material at URL, with additional Refs. 102–110, for detailed computational parameters and the results of geometry optimization using DFT+ U + J .
 - ⁶⁷ S.-j. Hu, S.-s. Yan, M.-w. Zhao, and L.-m. Mei, First-principles LDA+ U calculations of the co-doped ZnO magnetic semiconductor, *Phys. Rev. B* **73**, 245205 (2006).
 - ⁶⁸ H. J. Kulik and N. Marzari, Systematic study of first-row transition-metal diatomic molecules: A self-consistent DFT+ U approach, *The Journal of Chemical Physics* **133**, 114103 (2010).
 - ⁶⁹ K. Yu and E. A. Carter, Communication: Comparing ab initio methods of obtaining effective u parameters for closed-shell materials, *The Journal of Chemical Physics* **140**, 121105 (2014).
 - ⁷⁰ D. D. O’Regan, N. D. M. Hine, M. C. Payne, and A. A. Mostofi, Linear-scaling DFT + U with full local orbital optimization, *Phys. Rev. B* **85**, 085107 (2012).
 - ⁷¹ A. Ruiz-Serrano, N. D. M. Hine, and C.-K. Skylaris, Pulay forces from localized orbitals optimized in situ using a psinc basis set, *The Journal of Chemical Physics* **136**, 234101 (2012).
 - ⁷² D. D. O’Regan, M. C. Payne, and A. A. Mostofi, Subspace representations in ab initio methods for strongly correlated systems, *Phys. Rev. B* **83**, 245124 (2011).
 - ⁷³ Opium: the optimized pseudopotential interface unification module, <http://opium.sourceforge.net/>, accessed: 2017-11-30.
 - ⁷⁴ A. K. See and R. A. Bartynski, Electronic properties of ultrathin cu and fe films on $\text{tio}_2(110)$ studied by photoemission and inverse photoemission, *Phys. Rev. B* **50**, 12064 (1994).
 - ⁷⁵ H.-Y. Lee, S. J. Clark, and J. Robertson, Calculation of point defects in rutile tio_2 by the screened-exchange hybrid functional, *Phys. Rev. B* **86**, 075209 (2012).
 - ⁷⁶ A. Janotti, J. B. Varley, P. Rinke, N. Umezawa, G. Kresse, and C. G. Van de Walle, Hybrid functional studies of the oxygen vacancy in tio_2 , *Phys. Rev. B* **81**, 085212 (2010).
 - ⁷⁷ S. Gong and B.-G. Liu, Electronic structures and optical properties of TiO_2 : Improved density-functional-theory investigation, *Chinese Physics B* **21**, 057104 (2012).
 - ⁷⁸ Y. Zhang, J. W. Furness, B. Xiao, and J. Sun, Subtlety of tio_2 phase stability: Reliability of the density functional theory predictions and persistence of the self-interaction error, *The Journal of Chemical Physics* **150**, 014105 (2019).
 - ⁷⁹ P. Deák, B. Aradi, and T. Frauenheim, Quantitative theory of the oxygen vacancy and carrier self-trapping in bulk tio_2 , *Phys. Rev. B* **86**, 195206 (2012).
 - ⁸⁰ C. E. Patrick and F. Giustino, Gw quasiparticle bandgaps of anatase TiO_2 starting from DFT + U , *Journal of Physics: Condensed Matter* **24**, 202201 (2012).
 - ⁸¹ C. Persson and A. F. da Silva, Strong polaronic effects on rutile TiO_2 electronic band edges, *Applied Physics Letters* **86**, 231912 (2005).
 - ⁸² G. Mattioli, P. Alippi, F. Filippone, R. Caminiti, and A. Amore Bonapasta, Deep versus shallow behavior of intrinsic defects in rutile and anatase tio_2 polymorphs, *The Journal of Physical Chemistry C* **114**, 21694 (2010).
 - ⁸³ L. A. Agapito, S. Curtarolo, and M. Buongiorno Nardelli, Reformulation of DFT+ U as a pseudohybrid Hubbard density functional for accelerated materials discovery, *Phys. Rev. X* **5**, 011006 (2015).
 - ⁸⁴ M. Gallart, T. Cottineau, B. Hnerlage, V. Keller, N. Keller, and P. Gilliot, Temperature dependent photoluminescence of anatase and rutile tio_2 single crystals: Polaron and self-trapped exciton formation, *Journal of Applied Physics* **124**, 133104 (2018).
 - ⁸⁵ D. D. O’Regan, N. D. M. Hine, M. C. Payne, and A. A. Mostofi, Projector self-consistent DFT+ U using nonorthogonal generalized wannier functions, *Phys. Rev. B* **82**, 081102 (2010).
 - ⁸⁶ B. Huang, The screened pseudo-charge repulsive potential

- in perturbed orbitals for band calculations by DFT+U, *Phys. Chem. Chem. Phys.* **19**, 8008 (2017).
- ⁸⁷ G. Mattioli, F. Filippone, P. Alippi, and A. Amore Bonapasta, Ab initio study of the electronic states induced by oxygen vacancies in rutile and anatase TiO₂, *Phys. Rev. B* **78**, 241201 (2008).
 - ⁸⁸ V. I. Anisimov, F. Aryasetiawan, and A. I. Lichtenstein, First-principles calculations of the electronic structure and spectra of strongly correlated systems: the lda+u method, *Journal of Physics: Condensed Matter* **9**, 767 (1997).
 - ⁸⁹ M. T. Czyżyk and G. A. Sawatzky, Local-density functional and on-site correlations: The electronic structure of la₂cuo₄ and lacuo₃, *Phys. Rev. B* **49**, 14211 (1994).
 - ⁹⁰ G. Moynihan, G. Teobaldi, and D. D. O'Regan, Inapplicability of exact constraints and a minimal two-parameter generalization to the DFT+U based correction of self-interaction error, *Phys. Rev. B* **94**, 220104 (2016).
 - ⁹¹ O. K. Orhan and D. D. O'Regan, TDDFT+U: A critical assessment of the Hubbard *u* correction to exchange-correlation kernels and potentials, *Phys. Rev. B* **99**, 165120 (2019).
 - ⁹² Z. Hu and H. Metiu, Choice of U for DFT+U calculations for titanium oxides, *The Journal of Physical Chemistry C* **115**, 5841 (2011).
 - ⁹³ E. Finazzi, C. D. Valentin, G. Pacchioni, and A. Selloni, Excess electron states in reduced bulk anatase TiO₂: Comparison of standard GGA, GGA+U, and hybrid DFT calculations, *The Journal of Chemical Physics* **129**, 154113 (2008).
 - ⁹⁴ A. E. Bocquet, T. Mizokawa, K. Morikawa, A. Fujimori, S. R. Barman, K. Maiti, D. D. Sarma, Y. Tokura, and M. Onoda, Electronic structure of early 3d-transition-metal oxides by analysis of the 2p core-level photoemission spectra, *Phys. Rev. B* **53**, 1161 (1996).
 - ⁹⁵ N. A. Deskins and M. Dupuis, Electron transport via polaron hopping in bulk TiO₂: A density functional theory characterization, *Phys. Rev. B* **75**, 195212 (2007).
 - ⁹⁶ C. J. Calzado, N. C. Hernández, and J. F. Sanz, Effect of on-site coulomb repulsion term *u* on the band-gap states of the reduced rutile (110) TiO₂ surface, *Phys. Rev. B* **77**, 045118 (2008).
 - ⁹⁷ M. Nolan, S. D. Elliott, J. S. Mulley, R. A. Bennett, M. Basham, and P. Mulheran, Electronic structure of point defects in controlled self-doping of the TiO₂ (110) surface: Combined photoemission spectroscopy and density functional theory study, *Phys. Rev. B* **77**, 235424 (2008).
 - ⁹⁸ K. Yang, Y. Dai, B. Huang, and Y. P. Feng, Density-functional characterization of antiferromagnetism in oxygen-deficient anatase and rutile TiO₂, *Phys. Rev. B* **81**, 033202 (2010).
 - ⁹⁹ M. Kick, K. Reuter, and H. Oberhofer, Intricacies of dft+u, not only in a numeric atom centered orbital framework, *Journal of Chemical Theory and Computation* **15**, 1705 (2019).
 - ¹⁰⁰ H. J. Kulik and N. Marzari, A self-consistent Hubbard *u* density-functional theory approach to the addition-elimination reactions of hydrocarbons on bare feo+, *The Journal of Chemical Physics* **129**, 134314 (2008).
 - ¹⁰¹ D. Korotin, A. V. Kozhevnikov, S. L. Skornyakov, I. Leonov, N. Binggeli, V. I. Anisimov, and G. Trimarchi, Construction and solution of a wannier-functions based hamiltonian in the pseudopotential plane-wave framework for strongly correlated materials, *The European Physical Journal B* **65**, 91 (2008).
 - ¹⁰² E. Meagher and G. A. Lager, Polyhedral thermal expansion in the TiO₂ polymorphs; refinement of the crystal structures of rutile and brookite at high temperature, *The Canadian Mineralogist* **17**, 77 (1979).
 - ¹⁰³ M. Horn, C. F. Schwebdtferger, and E. P. Meagher, Refinement of the structure of anatase at several temperatures, *Zeitschrift für Kristallographie - Crystalline Materials* **136**, 273 (1972).
 - ¹⁰⁴ P. Giannozzi, S. Baroni, N. Bonini, M. Calandra, R. Car, C. Cavazzoni, D. Ceresoli, G. L. Chiarotti, M. Cococcioni, I. Dabo, A. D. Corso, S. de Gironcoli, S. Fabris, G. Fratesi, R. Gebauer, U. Gerstmann, C. Gougousis, A. Kokalj, M. Lazzeri, L. Martin-Samos, N. Marzari, F. Mauri, R. Mazzarello, S. Paolini, A. Pasquarello, L. Paulatto, C. Sbraccia, S. Scandolo, G. Sclauzero, A. P. Seitsonen, A. Smogunov, P. Umari, and R. M. Wentzcovitch, Quantum espresso: a modular and open-source software project for quantum simulations of materials, *Journal of Physics: Condensed Matter* **21**, 395502 (2009).
 - ¹⁰⁵ P. Giannozzi, O. Andreussi, T. Brumme, O. Bunau, M. B. Nardelli, M. Calandra, R. Car, C. Cavazzoni, D. Ceresoli, M. Cococcioni, N. Colonna, I. Carnimeo, A. D. Corso, S. de Gironcoli, P. Delugas, R. A. D. Jr, A. Ferretti, A. Floris, G. Fratesi, G. Fugallo, R. Gebauer, U. Gerstmann, F. Giustino, T. Gorni, J. Jia, M. Kawamura, H.-Y. Ko, A. Kokalj, E. Küçükbenli, M. Lazzeri, M. Marsili, N. Marzari, F. Mauri, N. L. Nguyen, H.-V. Nguyen, A. O. de-la Roza, L. Paulatto, S. Poncé, D. Rocca, R. Sabatini, B. Santra, M. Schlipf, A. P. Seitsonen, A. Smogunov, I. Timrov, T. Thonhauser, P. Umari, N. Vast, X. Wu, and S. Baroni, Advanced capabilities for materials modelling with quantum espresso, *Journal of Physics: Condensed Matter* **29**, 465901 (2017).
 - ¹⁰⁶ F. D. Murnaghan, The compressibility of media under extreme pressures, *Proceedings of the National Academy of Sciences of the United States of America* **30**, 244 (1944).
 - ¹⁰⁷ J. K. Burdett, T. Hughbanks, G. J. Miller, J. W. Richardson, and J. V. Smith, Structural-electronic relationships in inorganic solids: powder neutron diffraction studies of the rutile and anatase polymorphs of titanium dioxide at 15 and 295 k, *Journal of the American Chemical Society* **109**, 3639 (1987).
 - ¹⁰⁸ D. G. Isaak, J. D. Carnes, O. L. Anderson, H. Cynn, and E. Hake, Elasticity of TiO₂ rutile to 1800 k, *Physics and Chemistry of Minerals* **26**, 31 (1998).
 - ¹⁰⁹ W. Zhang, T. Hu, B. Yang, P. Sun, and H. He, The effect of boron content on properties of b-TiO₂ photocatalyst prepared by sol-gel method, *Journal of Advanced Oxidation Technologies* **16**, 261 (2013).
 - ¹¹⁰ V. Swamy and L. Dubrovinsky, Bulk modulus of anatase, *Journal of Physics and Chemistry of Solids* **62**, 673 (2001).

Supplementary Material to “First-principles Hubbard U and Hund’s J corrected approximate density-functional theory predicts an accurate fundamental gap in rutile and anatase TiO_2 ”

Okan K. Orhan¹ and David D. O’Regan¹

¹*School of Physics, AMBER, and CRANN Institute,
Trinity College Dublin, the University of Dublin, Ireland*

In this Supplementary Material, we describe an investigation into how the first-principles DFT+ U + J correction, when applied to both Ti 3*d* and O 2*p* subspaces, affects the predicted internal ionic geometry and equilibrium unit cell volume of rutile and anatase TiO_2 . We first, however, describe the Computational Details used overall, i.e., both here and in the main text.

I. COMPUTATIONAL DETAILS

Initial crystallographic information for TiO_2 -rutile and TiO_2 -anatase were adopted from Refs. 1 and 2. Norm-conserving scalar-relativistic LDA pseudo-potentials were produced using the pseudo-potential generator OPIUM³. Following transferability testing, a Ti^{3+} configuration with semi-core 3*s* and 3*p* orbitals in the valence and with relatively small, demanding cut-off radii of 1.54 a_0 (for *s*), 1.70 a_0 (*p*), and 1.82 a_0 (*d*), was chosen. Full geometry relaxation were performed with variable cell parameters at a high plane-wave cut-off energy E_{cut} (75 Ha or approximately 2040 eV) and automatically generated $3 \times 3 \times 5$ (TiO_2 -rutile) and $5 \times 5 \times 3$ (conventional-cell TiO_2 -anatase) Monkhorst-Pack Brillouin zone sampling grids using the Quantum Espresso (QE) code^{4,5}. The converged cell parameters were used to construct unfolded super-cells with 270 and 900 atoms, respectively, in order to emulate the same Brillouin zone sampling with real-valued Kohn-Sham orbitals within the ONETEP code⁶. This is a linear-scaling implementation of approximate KS-DFT using two nested optimization loops for the density kernel and a minimal set of non-orthogonal generalized Wannier functions (NGWFs)^{7,8}.

An under-pinning basis of $3^1 5^2 = 75$ *psinc* functions in all directions for TiO_2 -rutile (corresponding to the effective kinetic energy cut-offs of ~ 1776 eV, ~ 1776 eV, and ~ 1552 eV), and $3^1 5^2 = 75$ in the *x*- and *y*-directions and $3^1 7^2 = 147$ in *z*-direction for TiO_2 -anatase (corresponding to ~ 945 eV, ~ 945 eV, and ~ 1578 eV respectively), provided a basis set associated error of ≤ 1 meV in the total energy per atom. A total of 13 variationally optimized NGWFs initially centred on Ti atoms were used, to complete the second and third periods up to Kr, and a total 4 NGWFs variationally optimized NGWFs initially centred on O atoms to complete the period up to Ar. A converged, common NGWF cut-off radius of 12 a_0 was used for both species, with the same total energy tolerance. For the band gaps reported in the main

text but not here in the Supplementary Material, a second set of NGWFs, with the number and cut-off radii, where then added and variationally optimised, following Ref. 9, in order to reproduce the Kohn-Sham states around the conduction-band minimum. For Ti^0 NGWF initial guesses, this makes a only small improvement to the predicted gaps, typically on the order of 5 meV, but the effect is significant (order of 0.1 eV) for Ti^{3+} initial guesses. We emphasise that, for energies much above the conduction-band edges, the conduction band parts of the LDOS plots presented in the main text are qualitatively but not necessarily quantitatively reliable.

A discrete perturbation strength grid, $\delta\alpha^\uparrow = \{0, \pm 0.01, \pm 0.10, \pm 0.50, \pm 1.00\}$ eV was used to calculate the Hubbard U and Hund’s J parameters, without restarts in order to remove any risk of premature convergence declaration and hence under-estimated response. This was applied to a single spin channel only, following the 2×2 procedure introduced in Ref. 10. A smooth response was obtained for all matrix elements for both species, Ti 3*d* and O 2*p*, and for both crystal structures.

II. EFFECTS OF DFT+ U + J ON IONIC GEOMETRY

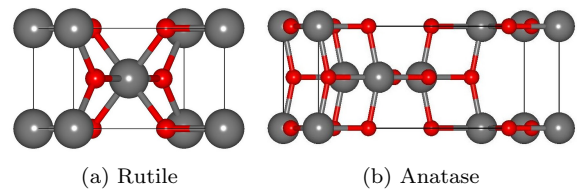


FIG. 1. Schematic crystal structures of TiO_2 -rutile and TiO_2 -anatase.

A. Geometry optimization procedure

For the purposes only of this Supplemental Material, the same QE LDA geometry optimization procedure was repeated for TiO_2 -rutile and TiO_2 -anatase, using 10^{-7} Ry, 10^{-5} Ry/Bohr and 10^{-10} Ry convergence thresholds for the total energy, forces for ionic minimization, and self-consistency, respectively, but with fixed lattice vectors corresponding to $\pm 1\%$ and $\pm 2\%$ isotropic strain. As ONETEP is not equipped to perform cell-wall stress calculations, these optimized, strained unit cells

were then repeated to form supercells with the same atom counts as before for each polymorph, in order to carry out ONETEP internal ionic geometry optimizations using DFT (LDA) and DFT+ $U+J$. In order to maintain a plane-wave equivalent real-space sampling of the supercell in ONETEP that remained commensurate with the unit-cell, however, it is necessary to conserve the number of real-space sampling (psinc) points. This means that, when a strain of $\pm x\%$ is applied, for $x \ll 1$, the equivalent plane-wave kinetic energy cut-off in each direction changes by a factor of $\approx \mp 2x\%$. While this effect is present to some extent in all plane-wave DFT codes, here it hampers more severely our ability to make precise conclusions as to the predicted unit cell volume.

Only the most successful DFT+ $U+J$ functional in terms of the band gap was tested, in the expedient form DFT+ $U_{\text{full}}^{d,p}$, $\alpha = J/2$. Only the first-principles parameters described in the main text were used, and we have not investigated the lattice volume dependence of the U and J parameters. Convergence thresholds of $5 \times 10^{-3} a_0$, 10^{-6} Ha, and 10^{-4} Ha a_0^{-1} were applied to the atomic displacement, total energy per atom, and maximum individual atomic force, respectively, within ONETEP. The energy versus volume data for each set of simulations were used to fit the Murnaghan equation-of-state¹¹, from which we extracted minimum-energy volumes and bulk moduli using a post-processing tool available within QE.

B. Structural information for TiO₂-rutile

For rutile, Fig. 2 indicates a close match between the energy, and separately the band gap, changes with respect to isotropic strain across LDA (two codes) and DFT+ $U+J$ (ONETEP, with fixed parameters). The total energies are not the same, differing by constants that are set to zero for illustrative purposes. The predicted band gap decreases with increasing lattice volume, albeit that this might feasibly not be the case if the parameters were made dependent upon the volume. Table I indicates that the small code dependence does not manifest in the internally relaxed bond lengths, and essentially that DFT+ $U+J$ closely preserves the internal geometry of this direct-gap system at its LDA parameters.

Table II confirms that DFT+ $U+J$ only marginally changes the predicted lattice volume and bulk modulus, subject to that caveat here that we cannot separately relax the three lattice vectors in ONETEP and we only explore isotropic strain with respect to the LDA (QE) relaxed unit cell. Remarkably, this result reflects those reported for very different, small molecular systems studied with a similar method in Ref. 10, where it was suggested that the O 2*p* correction compensates for Ti 3*d* correction in terms of the bonding strength and ionic forces. Finally, in order to compensate for discrepancy between the QE and ONETEP volumes, which most likely arises due to their differing plane wave grids (an approximate sphere of \mathbf{G} vectors in the former case, a cuboid in the latter

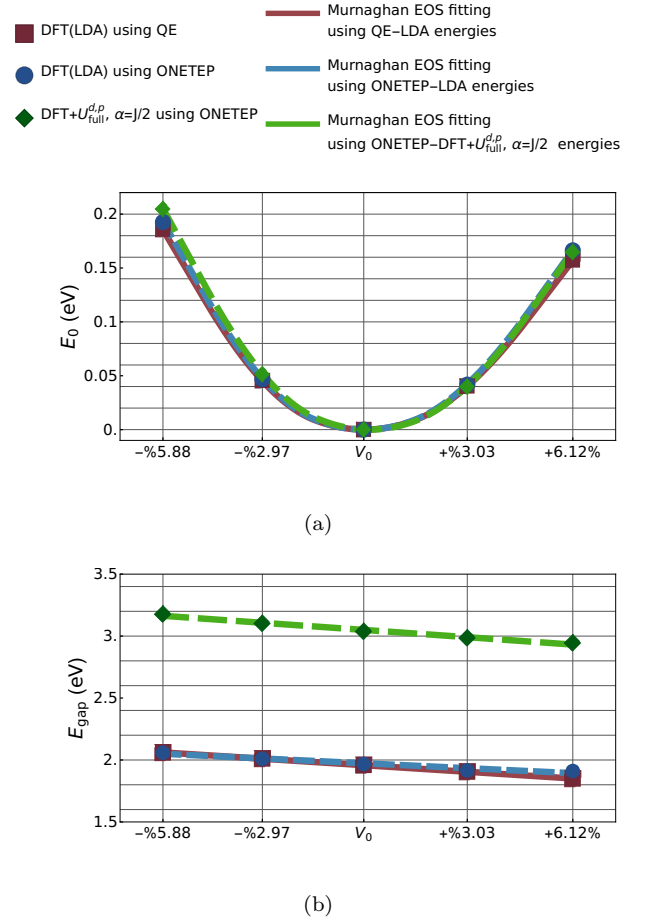


FIG. 2. (a) Total energies (per formula unit cell) as a function of isotropically-strained (QE LDA) lattice volume of TiO₂-rutile calculated using LDA within Quantum Espresso and ONETEP, and also using first-principles DFT+ $U+J$ within ONETEP, each with their respective converged internal ionic geometries. (b) The Kohn-Sham, or generalized Kohn-Sham, band gaps corresponding to (a) are shown here with respective linear fits. In the case of ONETEP data, there is an uncontrolled overestimation ~ 1 meV introduced here with respect to the results in the main text, due to non-optimization of conduction-band NGWFs.

case), we define the ‘code corrected’ as the Murnaghan interpolated DFT+ $U+J$ volume, multiplied by the ratio of the interpolated LDA (QE) and LDA (ONETEP) volumes. Extrapolating the band gap to this volume, and also applying the DFT+ $U+J$ conduction-band optimization correction calculated at the LDA (QE) geometry, we arrive at the DFT+ $U+J$ (corrected) band gap. For rutile, this is the same as the uncorrected result to the reasonable number of significant figures shown, which is also the same as the LDA (QE) geometry DFT+ $U+J$ shown in the main text. For rutile TiO₂, therefore, perhaps as a consequence of its direct band gap or relatively similar lattice vector lengths, the consequences for the geometry of changing the plane-wave code used, or changing from the LDA to first-principles DFT+ $U+J$ (with O 2*p*

Lattice vectors (a_0)			
\mathbf{v}_1^0	8.5289	0.0000	0.0000
\mathbf{v}_2^0	0.0000	8.5289	0.0000
\mathbf{v}_3^0	0.0000	0.0000	5.4729

Atomic positions (fractional)			
Ti	0.0000	0.0000	0.0000
Ti	0.5000	0.5000	0.5000
O	0.3040	0.3040	0.0000
O	0.6960	0.6960	0.0000
O	0.1960	0.8041	0.5000
O	0.8041	0.1960	0.5000

Bond lengths (a_0)		
	Ti – O (4 of)	Ti – O (2 of)
LDA (QE)	3.6160	3.6671
LDA (ONETEP)	3.6160	3.6671
DFT+ $U+J$	3.6141	3.6700
Experiment ¹²	3.6772	3.7349

TABLE I. Optimized zero-strain internal ionic geometries of TiO_2 -rutile, as predicted by two implementations of DFT (LDA) and by first-principles DFT+ $U+J$ in the guise of DFT+ $U_{\text{full}}^{d,p}$, $\alpha = J/2$, alongside experimental values for comparison. The QE LDA lattice vectors are used in all cases.

correction) are numerically small.

C. Structural information for TiO_2 -anatase

The procedure and data representation of the previous sub-section is repeated here for the case of anatase. In Table III, we first note that one of the lattice vectors is over twice the length of the others, which gives rise to a more significantly non-uniform equivalent plane-wave grid in ONETEP. Nonetheless, as the potential is well converged, we note only a small difference in internally-relaxed LDA bond lengths of QE and ONETEP. The change to DFT+ $U+J$ makes a larger but still small change, and does not significantly improve the bond lengths with respect to their experimental values.

Turning next to, Fig. 3, we observe that for anatase the effect of the DFT+ $U+J$ correction on the predicted equilibrium lattice volume (subject always to the caveat that only isotropic strain is considered) is rather small compared to the effect of changing the code. We expect that this arises due to the aforementioned more significant dependence of the effective plane-wave cut-off energy on the lattice volume in ONETEP, when compared to QE, which is made more apparent due to the very anisotropic lattice vectors of anatase. Again, as the potential is well

	V_0^{fit} (a_0^3)	% Error	K (GPa)
LDA (QE)	398.26	-5.50	256.8
LDA (ONETEP)	398.27	-5.50	269.9
DFT+ $U+J$	398.69	-5.40	276.8
DFT+ $U+J$ (corrected)	398.68	-5.40	-
Experiment ¹³	421.43 ^a	-	211.5 ^a

Evaluated at V_0	E_{gap} (eV)	$dE_{\text{gap}}^{\text{fit}}/dV$ (eV a_0^{-3})
LDA (QE)	1.96	-4.4×10^{-3}
LDA (ONETEP)	1.97	-3.3×10^{-3}
DFT+ $U+J$	3.04	-4.9×10^{-3}
DFT+ $U+J$ (corrected)	3.04	-

TABLE II. Estimated minima V_0^{fit} of Murnaghan equation of state, as fitted to the ground-state energies of TiO_2 -rutile using LDA within QE, and using LDA and DFT+ $U+J$ within ONETEP (top panel), and in all cases based on strained LDA (QE) lattice vectors but with internal ionic coordinates relaxed with the stated functional. The percentage volume error with respect to experiment is provided, as well as an estimate of the bulk modulus (K). Also shown are the calculated band gaps for the internally-relaxed geometry at the LDA (QE) volume V_0 , as well as the slope of the band gap with respect to volume as extracted from a linear fit. DFT+ $U+J$ (corrected) values are our best estimate, as extrapolated using the linear fit based on the ‘code corrected’ DFT+ $U+J$ volume described in the text, and applying the known correction constant for conduction-band edge optimization calculated at the LDA (QE) geometry.

converged, the effect on the LDA band gap of changing the code is small. The predicted gaps decrease with lattice volume, but at a lower rate than that found which we observed in rutile.

Turning finally to Table IV, we note that DFT+ $U+J$ causes an expansion of the volume in anatase, when the code is approximately corrected for, and although this is, as for rutile, a change in the direction of the experimental value, the change is very small. When internal geometric relaxation is included, with the LDA (QE) lattice vectors, the predicted DFT+ $U+J$ band gap increases by 0.06 eV with respect to the value reported in the main text, or by 0.04 eV when anisotropic plane-wave basis and conduction-band optimization related errors are approximately corrected. This takes us further from the most reliable available experimental fundamental gap value of 3.47 eV, and, noting that the bond lengths change only marginally, it is not clear whether this due to a genuine geometry relaxation effect on the gap. Alternative possibilities include a gap-preserving shift in indirect band edge wave-vectors, which would result in the approximately sampled gap spuriously opening, or the

Lattice vectors (a_0)			
\mathbf{v}_1^0	7.0131	0.0000	0.0000
\mathbf{v}_2^0	0.0000	7.0131	0.0000
\mathbf{v}_3^0	0.0000	0.0000	17.7311

Atomic positions (fractional)			
Ti	0.0000	0.2500	0.3750
Ti	0.0000	0.7500	0.6250
Ti	0.5000	0.7500	0.8750
Ti	0.5000	0.2500	0.1250
O	0.0000	0.2500	0.1670
O	0.0000	0.7500	0.8330
O	0.5000	0.7500	0.6670
O	0.5000	0.2500	0.3330
O	0.0000	0.7500	0.4170
O	0.0000	0.2500	0.5830
O	0.5000	0.7500	0.0830
O	0.5000	0.2500	0.9170

	Bond lengths (a_0)	
	Ti – O (4 of)	Ti – O (2 of)
LDA (QE)	3.5851	3.6865
LDA (ONETEP)	3.5851	3.6855
DFT+ $U+J$	3.5898	3.6642
Experiment ¹²	3.6513	3.7394

TABLE III. Optimized zero-strain internal ionic geometries of TiO_2 -anatase, as predicted by two implementations of DFT (LDA) and by first-principles DFT+ $U+J$ in the guise of DFT+ $U_{\text{full}}^{d,p}$, $\alpha = J/2$, alongside experimental values for comparison. The QE LDA lattice vectors are used in all cases.

real-space grid points shifting to locations where some of the DFT+ $U+J$ projectors have a greater amplitude, again giving rise to an increased gap. The former effect would be identified by non-self-consistent band-structure interpolation, were it technically available, and the latter effect, if present, might be mitigated by geometry self-consistent calculated U and J parameters.

Overall, subject to the technical limitations of our study, we can tentatively conclude that in the systems investigated, first-principles DFT+ $U+J$ with O $2p$ correction makes only a marginal change to the ionic geometries of the underlying LDA, and that the effects of changing the DFT code used can be more significant. As we have developed a prescription for exactly emulating DFT+ $U+J$ for closed-shell systems in codes with no Hund’s J implementation (using the parameters $U_{\text{full}} = U - 2J$ and $\alpha = J/2$), the stage is now set for future, lattice and internal geometry self-consistent DFT+ $U+J$ calculations with finely sampled band-structures.

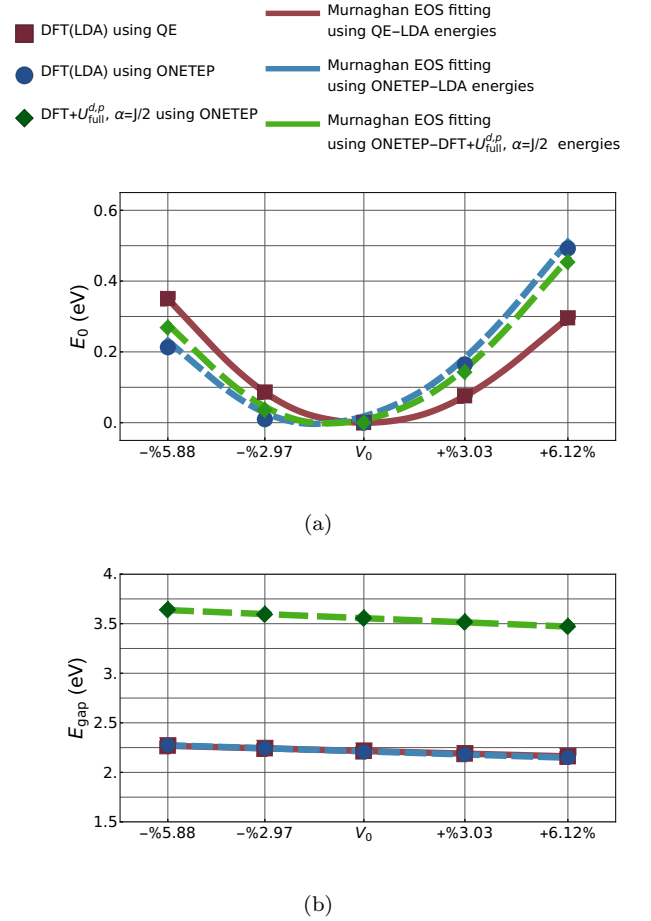


FIG. 3. (a) Total energies (per formula unit cell) as a function of isotropically-strained (QE LDA) lattice volume of TiO_2 -anatase calculated using LDA within Quantum Espresso and ONETEP, and also using first-principles DFT+ $U+J$ within ONETEP, each with their respective converged internal ionic geometries. (b) The Kohn-Sham, or generalized Kohn-Sham, band gaps corresponding to (a) are shown here with respective linear fits. In the case of ONETEP data, there is an uncontrolled overestimation ~ 1 meV introduced here with respect to the results in the main text, due to non-optimization of conduction-band NGWFs.

	V_0^{fit} (\AA^3)	% Error	K (GPa)
LDA (QE)	872.52	-4.89	220.9
LDA (ONETEP)	860.45	-6.20	253.2
DFT+ U + J	864.09	-5.81	255.3
DFT+ U + J (corrected)	876.21	-4.49	
Experiment	917.37 ¹⁴	-	178 ¹⁵

Evaluated at V_0	E_{gap} (eV)	$dE_{\text{gap}}^{\text{fit}}/dV$ (eV \AA^{-3})
LDA (QE)	2.22	- 1.0×10^{-3}
LDA (ONETEP)	2.21	- 1.2×10^{-3}
DFT+ U + J	3.56	- 1.6×10^{-3}
DFT+ U + J (corrected)	3.54	-

TABLE IV. Estimated minima V_0^{fit} of Murnaghan equation of state, as fitted to the ground-state energies of TiO_2 -anatase using LDA within QE, and using LDA and DFT+ U + J within ONETEP (top panel), and in all cases based on strained LDA (QE) lattice vectors but with internal ionic coordinates relaxed with the stated functional. The percentage volume error with respect to experiment is provided, as well as an estimate of the bulk modulus (K). Also shown are the calculated band gaps for the internally-relaxed geometry at the LDA (QE) volume V_0 , as well as the slope of the band gap with respect to volume as extracted from a linear fit. DFT+ U + J (corrected) values are our best estimate, as extrapolated using the linear fit based on the ‘code corrected’ DFT+ U + J volume described in the text, and applying the known correction constant for conduction-band edge optimization calculated at the LDA (QE) geometry.

- ¹ E. Meagher and G. A. Lager, *The Canadian Mineralogist* **17**, 77 (1979).
- ² M. Horn, C. F. Schwebdtferger, and E. P. Meagher, *Zeitschrift für Kristallographie - Crystalline Materials* **136**, 273 (1972).
- ³ “Opium:the optimized pseudopotential interface unification module,” <http://opium.sourceforge.net/>, accessed: 2017-11-30.
- ⁴ P. Giannozzi, S. Baroni, N. Bonini, M. Calandra, R. Car, C. Cavazzoni, D. Ceresoli, G. L. Chiarotti, M. Cococcioni, I. Dabo, A. D. Corso, S. de Gironcoli, S. Fabris, G. Fratesi, R. Gebauer, U. Gerstmann, C. Gougoussis, A. Kokalj, M. Lazzeri, L. Martin-Samos, N. Marzari, F. Mauri, R. Mazzarello, S. Paolini, A. Pasquarello, L. Paulatto, C. Sbraccia, S. Scandolo, G. Sciauzero, A. P. Seitsonen, A. Smogunov, P. Umari, and R. M. Wentzcovitch, *Journal of Physics: Condensed Matter* **21**, 395502 (2009).
- ⁵ P. Giannozzi, O. Andreussi, T. Brumme, O. Bunau, M. B. Nardelli, M. Calandra, R. Car, C. Cavazzoni, D. Ceresoli, M. Cococcioni, N. Colonna, I. Carnimeo, A. D. Corso, S. de Gironcoli, P. Delugas, R. A. D. Jr, A. Ferretti,

- A. Floris, G. Fratesi, G. Fugallo, R. Gebauer, U. Gerstmann, F. Giustino, T. Gorni, J. Jia, M. Kawamura, H.-Y. Ko, A. Kokalj, E. Küçükbenli, M. Lazzeri, M. Marsili, N. Marzari, F. Mauri, N. L. Nguyen, H.-V. Nguyen, A. O. de-la Roza, L. Paulatto, S. Poncé, D. Rocca, R. Sabatini, B. Santra, M. Schlipf, A. P. Seitsonen, A. Smogunov, I. Timrov, T. Thonhauser, P. Umari, N. Vast, X. Wu, and S. Baroni, *Journal of Physics: Condensed Matter* **29**, 465901 (2017).
- ⁶ J. C. A. Prentice, J. Aarons, J. C. Womack, A. E. A. Allen, L. Andrinopoulos, L. Anton, R. A. Bell, A. Bhandari, G. A. Bramley, R. J. Charlton, R. J. Clements, D. J. Cole, G. Constantinescu, F. Corsetti, S. M.-M. Dubois, K. K. B. Duff, J. M. Escartín, A. Greco, Q. Hill, L. P. Lee, E. Linscott, D. D. O’Regan, M. J. S. Phipps, L. E. Ratcliff, A. R. Serrano, E. W. Tait, G. Teobaldi, V. Vitale, N. Yeung, T. J. Zuehlsdorff, J. Dziedzic, P. D. Haynes, N. D. M. Hine, A. A. Mostofi, M. C. Payne, and C.-K. Skylaris, *The Journal of Chemical Physics* **152**, 174111 (2020).
- ⁷ C.-K. Skylaris, P. D. Haynes, A. A. Mostofi, and M. C. Payne, *The Journal of Chemical Physics* **122**, 084119

- (2005).
- ⁸ P. D. Haynes, C.-K. Skylaris, A. A. Mostofi, and M. C. Payne, *physica status solidi (b)* **243**, 2489 (2006).
 - ⁹ L. E. Ratcliff, N. D. M. Hine, and P. D. Haynes, *Phys. Rev. B* **84**, 165131 (2011).
 - ¹⁰ E. B. Linscott, D. J. Cole, M. C. Payne, and D. D. O'Regan, *Phys. Rev. B* **98**, 235157 (2018).
 - ¹¹ F. D. Murnaghan, *Proceedings of the National Academy of Sciences of the United States of America* **30**, 244 (1944).
 - ¹² J. K. Burdett, T. Hughbanks, G. J. Miller, J. W. Richardson, and J. V. Smith, *Journal of the American Chemical Society* **109**, 3639 (1987).
 - ¹³ D. G. Isaak, J. D. Carnes, O. L. Anderson, H. Cynn, and E. Hake, *Physics and Chemistry of Minerals* **26**, 31 (1998).
 - ¹⁴ W. Zhang, T. Hu, B. Yang, P. Sun, and H. He, *Journal of Advanced Oxidation Technologies* **16**, 261 (2013).
 - ¹⁵ V. Swamy and L. Dubrovinsky, *Journal of Physics and Chemistry of Solids* **62**, 673 (2001).